Version of Record: https://www.sciencedirect.com/science/article/pii/S0003267021009508
Manuscript_70fe1248ddc9b8c2e63681a76381a4ae

Electrochemical detection of Dopamine with Negligible Interference from Ascorbic and Uric acid by means of Reduced Graphene Oxide and metals-NPs based electrodes

Bernardo Patella[a], Alessia Sortino[a], Francesca Mazzara[a], Giuseppe Aiello[a], Giuseppe Drago[a], Claudia Torino[b], Antonio Vilasi[b], Alan O'Riordan[c], Rosalinda Inguanta[a]

[a]Dipartimento di Ingegneria, Università degli Studi di Palermo;

[b]Istituto di Fisiologia Clinica (IFC)-Consiglio Nazionale delle Ricerche-Reggio Calabria-Italy

[c]Nanotechnology group, Tyndall National Institute, University College Cork, Dyke Parade, Cork, Ireland.

ABSTRACT

Dopamine is an important neurotransmitter involved in many human biological processes as well as in different neurodegenerative diseases. Monitoring the concentration of dopamine in biological fluids, i.e., blood and urine is an effective way of accelerating the early diagnosis of these types of diseases. Electrochemical sensors are an ideal choice for real-time screening of dopamine as they can achieve fast, portable inexpensive and accurate measurements. In this work, we present electrochemical dopamine sensors based on reduced graphene oxide coupled with Au or Pt nanoparticles. Sensors were developed by co-electrodeposition onto a flexible substrate, and a systematic investigation concerning the electrodeposition parameters (concentration of precursors, deposition time and potential) was carried out to maximize the sensitivity of the dopamine detection. Square wave voltammetry was used as an electrochemical technique that ensured a high sensitive detection in the nM range. The sensors were challenged against synthetic urine in order to simulate a real sample detection scenario where dopamine concentrations are usually lower than 600 nM. Our sensors show a negligible interference from uric and ascorbic acids which did not affect sensor performance. A wide linear range (0.1–20 µm for gold nanoparticles, 0.1–10 µm for platinum nanoparticles) with high sensitivity (6.02 and 7.19 µA μM^{-1} cm^{-2} for gold and platinum, respectively) and a low limit of detection (75 and 62 nM for Au and Pt, respectively) were achieved. Real urine samples were also assayed, where the concentrations of dopamine detected aligned very closely to measurements undertaken using conventional laboratory techniques. Sensor fabrication employed a cost-effective production process with the possibility of also being integrated into flexible substrates, thus allowing for the possible development of wearable sensing devices.

KEYWORDS: dopamine, electrochemical sensor, neurodegenerative disease, graphene oxide, metal nanoparticles, urine.

1 Introduction

Among the neurotransmitters released from the brain, dopamine (DA) is the most important because of its involvement in many different biological processes such as memory, sleep, mood and learning. In addition, variation of DA concentrations in human body fluids has been recently related to some neurodegenerative diseases, such as Alzheimer's and Parkinson's diseases [1–3]. Alzheimer's disease [4] arises from the formation of amyloid plaques that hinder the DA-ergic neurons and consequently their capability to produce DA. Parkinson's, the second most common neurodegenerative disease, is linked to the degeneration of the nerve cells of the basal ganglia (*substantia nigra*) of the brain [5], which results in a decrease of DA production. DA is also related to hyperactivity and attention deficit hyperactivity disorder (ADHD) found in children [6]. ADHD is attributable to the alterations in some specific areas of the brain (pre-frontal cortex, part of the cerebellum and some of the basal ganglia, clusters of nerve cells located deep in the brain) that regulate attention and which are smaller in people with this disorder. For each disease and patient, there are different combinations of symptoms and prescribed drug therapy must be carefully tailored to meet the individual needs of a patient [7]. The first goal of pharmacological therapies is to restore optimal level of DA production and then, to maintain it over time. Consequently, it is necessary to continuously balance the drug therapy by constantly monitoring the DA concentrations.

As such, the possibility of applying a rapid detection system for this important neurotransmitter in human body fluids, such as blood and urine, is of extreme importance not only for balancing drug therapy but also for early disease diagnoses [8].

Nowadays, DA is detected by enzyme linked immuno-sorbet assay (ELISA) [9] and high pressure liquid chromatography (HPLC) [10] each achieving different limits of detection (LOD, 0.05 µM in urine and 0.5 µM in plasma). Despite the high sensitivity of these techniques, they are expensive, lab based difficult to handle, time consuming and require highly skilled laboratory personnel to operate them. These drawbacks can make DA screening troublesome and difficult. Electrochemical methods are ideal candidates to overcome these drawbacks [11–15], particularly if integrated into wearable sensors [16,17]. Indeed, just a simple compact potentiostat (low cost portable device [18]) is enough to obtain a portable sensing device, eliminating the need for bulky lab-based HPLC or ELISA systems [19]. In addition, electrode fabrication is cost-effective, reproducible and the as-fabricated sensors are good enough to compete with the traditional lab-based techniques [20–23]. For DA detection, the main disadvantage of electrochemical sensors is the interference from uric (UA) and ascorbic acid (AA). Both acids are present in all biological fluids at high concentrations and, unfortunately, have redox potential close to DA [24,25], complicating its selective detection. To overcome these problems, it is necessary chemically modify an electrode with a material that has a high selectivity towards DA. It has been reported that graphene based electrodes have excellent electrocatalytic properties for a selective detection of DA even in the presence of interfering species [26,27]. In particular, graphene oxide (GO) and its reduced form (rGO) have been widely used as an active material for sensors fabrication [28–30]. Their success in this field is due to the high surface area, good electric conductivity, mechanical stability and the presence of various functional groups, ie hydroxyl, carboxyl and epoxy groups [31,32].

Different metal nanoparticles (NPs) have been used to modify GO and rGO with the aim of improving their performance [33–35], in terms of surface area, electrical and thermal conductivity, stability and electrocatalytic efficiency [36–38]. In the case of DA detection [39,40], rGO combined with Au or Pt NPs ensures excellent electrical conductivity, stability and electrocatalytic properties as well as biocompatibility [41,42]. The main approach to producing NPs-rGO electrodes consists of the separated synthesis of NPs and rGO followed by their mixing to form a composite [43,44]. This process is time-consuming and difficult because each step must be carefully controlled. Recently, one step electrochemical reduction of both metal precursor and GO has been demonstrated [45]. This is an important approach for the synthesis of NPs-rGO based electrodes because it is easily undertaken, cost effective, rapid and does not require any particular chemical treatment.

Here, starting from the preliminary results reported in our recent work [23], we have simultaneously deposited, onto an ITO-PET substrate, AuNPs-rGO and PtNPs-rGO to develop a flexible, cheap and biocompatible electrode suitable for DA detection. A systematic investigation of the electrochemical parameters that control the fabrication process of the sensors was carried out, with the aim to maximize both the sensitivity and linear dynamic range. The AuNPs-rGO and PtNPs-rGO based electrodes have been previously investigated [11,27,35,39,46], but here we integrate them into a flexible, light and transparent substrate that allows not only wearable applications but they may also be easily integrated into urine collection bags. Such an approach would allow continuous and non-invasive monitoring in bedridden patients, severely affected by neurodegenerative diseases, which is the ultimate goal of our research project. To validate the possible use of the sensors for the detection of DA in urine, the sensor performance was first studied in synthetic urine (completely identical to real samples) to understand the influence of a such complex matrix on sensor performance. Following this, DA was quantified in real urine samples where the sensor results were observed to be comparable with those obtained using standard HPLC technique.

2 Experimental

2.1 Fabrication and characterization of sensors

As substrate for the co-deposition of metal NPs and rGO, sheets of ITO-PET (indium tin oxide/ polyethylene terephthalate) with 60 Ω cm^{-2} sheet resistance were used (Sigma Aldrich). This substrate was selected because is flexible, commercially available at low price and has good chemical and mechanical properties. All reagents (graphene oxide (solution 4mg/mL), phosphate buffer solution (PBS, pH 7.4), acetate buffer solution (ABS, pH 5.4), $KAuCl_4$ (98%), ethanol (96%), acetic acid (100%), sodium acetate (99%), K_2PtCl_6 (98%), dopamine hydrochloride (98%), uric acid (99%) and ascorbic acid (99%)) were purchased from Sigma Aldrich and used as received and diluted in deionized water (Type 1, resistivity > 18 MΩ·cm). Commercially available synthetic urine (Sigma Aldrich) was also used to simulate the operation of the sensors in real conditions and to understand the influence of a such complex matrix on sensor performance. Electrochemical depositions were carried out in a three-electrode cell with a saturated calomel electrode (SCE) as reference and a Pt wire as counter electrode using a PAR potentiostat/galvanostat (PARSTAT, mod. 2273). Electrodes were mounted into a home-made cell, made in acrylonitrile-butadiene-styrene, fabricated by a 3D printing (Zortrax M200), having a volume of 1 mL and a working electrode area of about 0.785 cm^2. Details on cell configuration can be found in [47]. Prior to deposition of NPs and rGO, the ITO-PET substrate was ultrasonically cleaned in pure iso-propanol for 15 min and then rinsed with deionized water. In order to prepare the deposition bath, GO and Au or Pt precursor were diluted in ABS at different concentrations. Deposition was also carried out after dissolving the chemicals in PBS. The results showed a negligible difference in the electrode behaviour, but the morphology of the electrode was more uniform using ABS, as confirmed by FESEM images (Figure S1A and S1B). Therefore, ABS was selected as buffer for the deposition step. The effect of the concentration of metal precursor (from 0.025 mM to 5 mM) and GO (from 0.25 to 1 mg/mL), the influence of the deposition time (from 50 to 300 sec) and potential (from -0.4 to -1 V vs SCE) were investigated in order to determine the optimal deposition conditions. For each experiment, 0.8 mL of a fresh solution was used. A constant cathodic potential was applied for each time using ITO-PET as a working electrode. For each investigated parameter, electrodes were employed for DA detection and the best deposition conditions selected. A stock DA solution was prepared by diluting dopamine hydrochloride in 0.01 mM HCl (pH 5). The acidic condition is necessary to guarantee DA dissolution and solution stability, which is known to be highly affected by pH [48]. In fact, we found that in the DA solutions with pH > 5, after 24 h of storing at 4 °C, black particulates were formed due to DA oxidation to quinoid form [49].

Modified electrodes were characterized by field emission scanning electron microscopy (FESEM, FEG-ESEM, FEI QUANTA 200) equipped with energy dispersive spectroscopy (EDS), X-ray diffraction, micro-Raman spectroscopy and X-ray photoelectron Spectroscopy (XPS). The characterization methods are detailed in previous works [50–55]. To verify the homogeneity of the obtained electrodes, FESEM and EDS were carried out in different areas. X-ray (RIGAKU, D-MAX 25600 HK) diffraction patterns were obtained using Ni-filtered Cu Kα radiation (λ = 1.54 Å) with a tube voltage and current of 40 kV and 100 mA, respectively. Raman was performed using a He:Ne laser (633 nm) calibrated by the Raman peak of polycrystalline Si (520 cm^{-1}). Raman spectra and diffraction patterns were analysed by comparison with literature data. The modified ITO-PET electrodes were also investigated by XPS that was performed using a ULVAC-PHI PHI 5000 Versa Probe II Scanning XPS Microprobe™, equipped with a Al Kα (1486.6 eV) source in a FAT mode. The high resolution XPS spectra of Au 4f and C 1s were collected with the 128 channels hemispherical analyser at the pass energy of 23.5 eV and energy step size of 0.05 eV. Au 4f at 83.95 ± 0.05 eV was used to calibrate the binding energy (BE) scale.

2.2 Sensor Performance

For the characterization of the sensor performance, the same electrochemical cell described above was used. In this cell NPs-rGO-ITO acted as a working electrode, Pt wire as counter and SCE as reference electrodes. To explore possible fouling phenomena of electrode during the DA detection, the sensors were characterized with cyclic voltammetry (CV) tests. CV was carried out in PBS containing DA 100 μM, in the potential range from -0.5 V to 0.5 V vs SCE with a scan rate of 25 mV/sec, for 30 cycles. CV tests at different scan rates were also carried out to evaluate the double layer capacitance (C_{dL}) of the electrodes. Tests were performed in the range potential from 0.0 to 0.2 V vs SCE (i.e., in the non-faradaic region) in PBS and at room temperature.

Square wave voltammetry (SWV) was performed in the range potential from -0.5 to 0.8V vs. SCE, with a pulse of 0.025 V for 0.02 sec and a step height of 1 mV. SWV was used as the electrochemical technique for DA detection because of its higher sensitivity, compared to linear sweep voltammetry (LSV), and differential pulse voltammetry (DPV). This was confirmed by the results given in Figure S1C, where the detection peak of DA 30 μM using SWV and LSV, respectively, is presented. It was observed that the SWV peak intensity of DA was almost 10 times higher than the other techniques, thereby confirming the superior sensitivity of SWV which was used going forwards. To address the effect of rGO and metal NPs, the ITO substrate was electrochemically characterized both prior to and after the deposition of these materials. The sensor was calibrated using a blank solution of PBS, pH 7.4, close to physiological one. In the blank solution, different amounts of DA were added and the electrode was calibrated making 5 different replicates for each concentration. The selectivity of the sensor for DA was assessed in the presence of different concentration of AA and UA. In particular, to simulate the worst possible case, the selectivity was verified using very high concentration of interferents (from 10 to 500 μM for AA, and from 10 to 2000 μM for UA) [56,57].

To further validate the sensors, real urine samples were collected for 24 h and were tested in an authorized analysis laboratory where the standard HPLC method was used. In particular, the same urine sample was tested to quantify DA using both HPLC and our sensor, in order to compare the results. For the electrochemical detection, the urine samples were diluted (50% in volume) with PBS and tested without any pre-treatment.

For each experiment, a new electrode with the same features was used, making three or five replicate tests. GraphPad Prism 6.0 software was used to perform statistical analysis and the data were reported as mean ± standard deviation. Differences were recognized using one-way repeated measures ANOVA with Bonferroni post hoc test, and were considered significant those with $P < 0.05$.

3 Results and Discussion

3.1 Fabrication and characterization of sensors

The active material for the fabrication of the sensors is based on reduced graphene oxide (rGO) and gold nanoparticles (AuNPs) obtained by electrochemical co-deposition. In particular, the deposition reactions are:

$$GO + xH^+ + ye^- \rightarrow rGO + zH_2O \qquad (1)$$

$$AuCl_4^- + 3e^- \rightarrow Au + 4Cl^- \qquad (2)$$

While the deposition mechanism of gold is well known, that of rGO is still under study, and the reaction reported here is the the most commonly accepted [58,59]. In our appraoch, these reactions led to simultaneous deposition of rGO micro-sheets uniformly covered with Au nanoparticles on the entire area of electrodes discussed below.

We first verified if the electrodes proposed herein should to be employed as disposable sensors only. The electrochemical DA detection occurs by its oxidation, leading to the formation a poly-dopamine (PDA, see the electro-polymerization mechanism reported in Figure S2) on the substrate [60,61]. Thus, it is plausible that a fouling process of the electrode surface may occur that would subsequently inhibit its reactivity and thus sensitivity towards DA detection. To verify this possibility, an initial CV study was carried out using AuNPs-rGO-ITO in PBS in the presence of 100 µM DA.

CV curves reported in Figure 1, confirmed our hypothesis. Two paired peaks at 0.08/0.16 V and -0.37/-0.27 vs SCE, attributed to the oxidation of DA in dopaminequinone and leucodopaminechrome in dopaminechrome, respectively [61], are present. In particular, the peak at 0.08 V decreases with increasing CV cycles. After 5 and 30 cycles, the peak current intensities decrease by ~ 10% and ~20%, respectively (Figure S3). This arises due to the formation of a polydopamine layer that then hinders further electrochemical oxidation of DA at the electrode interface. This phenomenon happens with both AuNPs and PtNPs and confirms electrode fouling, as demonstrated by EDS and FESEM analyses performed on the electrode surface after CV test (Figure S4). In particular, the EDS shows the presence of N peak while in the FESEM images a low conductive layer was observed, both attributable to the polydopamine deposition. To this end, each experiment in this work was carried out with a fresh electrode, and to verify reproducibility, each test was performed using 3 or 5 different replicates. However, it is important to highlight that the electrode does not lose its functionality, in fact, after the 30 CV cycles they are still able to detect the concentration of dopamine although with a lower sensitivity (Figure S5).

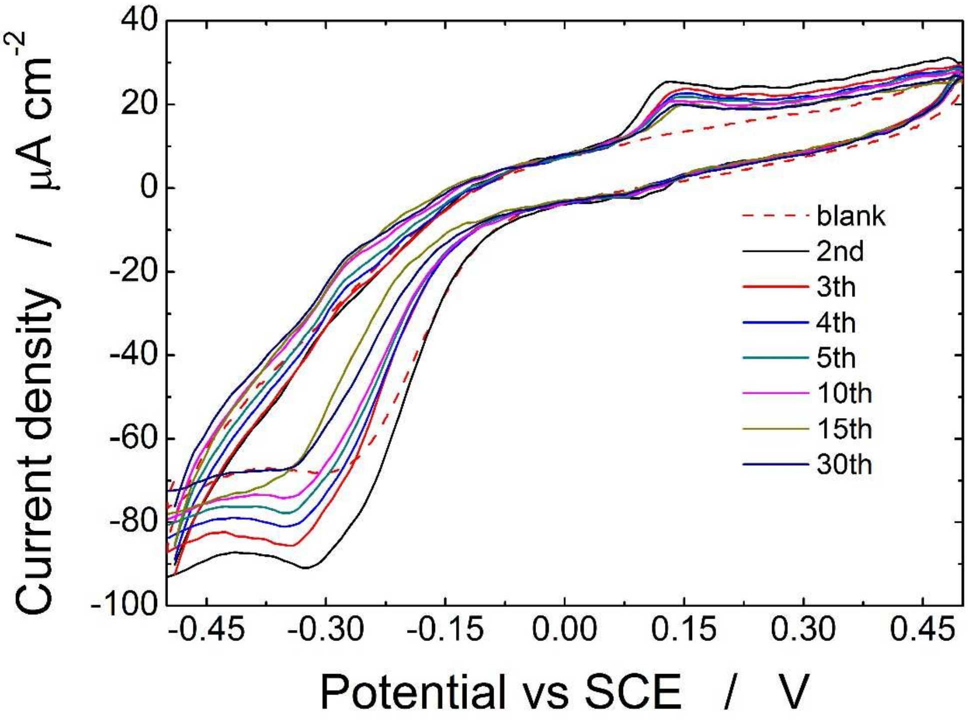

Figure 1. CV curves in the presence of 100 μm of DA using AuNPs-rGO-ITO based sensors.

The single effect of rGO and Au NPs on the surface of electrode was studied and the results are showed in Figure 2. In particular, results for bare ITO, ITO modified with Au-NPs (AuNPs-ITO), ITO modified with rGO (rGO-ITO) and ITO modified with both rGO and AuNPs (AuNPs-rGO-ITO) are presented.

Figure 2A shows the SWV curves for the detection of 25 μM of DA using the progressively modified ITO substrate. From these curves the values of peak current density (black) and peak potential (blue) were calculated and reported in Figure 2B. As predictable, due to the low electrocatalytic efficiency, the peak current density of DA detection using bare ITO is very low and occurs at more positive potential compared to the electrode with rGO and AuNPs separately. When both NPs and rGO are co-deposited into the electrode, the peak current density of DA is higher and the peak potential is lower compared to the ITO modified with these materials separately. It means that the electrode shows improved properties than just the sum of the properties of rGO and Au-NPs, although the major effect can be attributed to the presence of rGO. In fact, with respect to the value measured for bare ITO, the peak current density in the presence of only rGO increases by ~200%, while for Au NPs an increase of only ~26% was obtained. In the presence of Au NPs, the observed signal enhancement is due to their high conductivity and also increased electrochemical active surface area [62]. The high rGO electrocatalytic activity towards the DA detection is attributable to the π–π interactions between the aromatic structure of the GO and DA molecules that ensures a faster electron transfer rate [27]. These experiments clearly show that the modification of the electrode with rGO and AuNPs is a good approach to increase the sensitivity of the electrode. This is due to the synergistic effect of the simultaneous presence of Au NP and rGO, which synergistically improve the electrochemical properties and the catalytic activity and provide a large surface area for the reaction of the electroactive molecules. In addition, as reported in [64], the functional groups of rGO stabilize the AuNPs improving the durability of the catalyst.

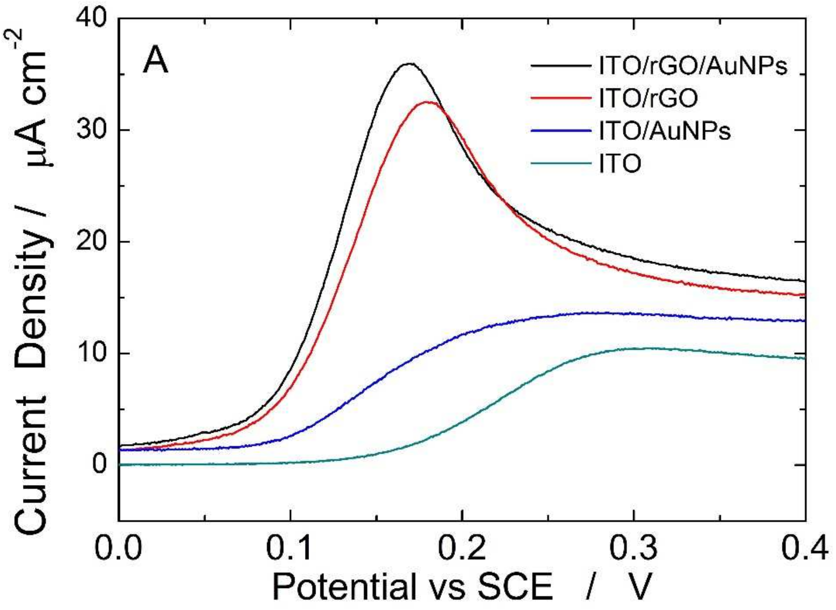
A
ITO/rGO/AuNPs
ITO/rGO
ITO/AuNPs
ITO
Current Density / μA cm^{-2}
Potential vs SCE / V
40
30
20
10
0
0.0
0.1
0.2
0.3
0.4

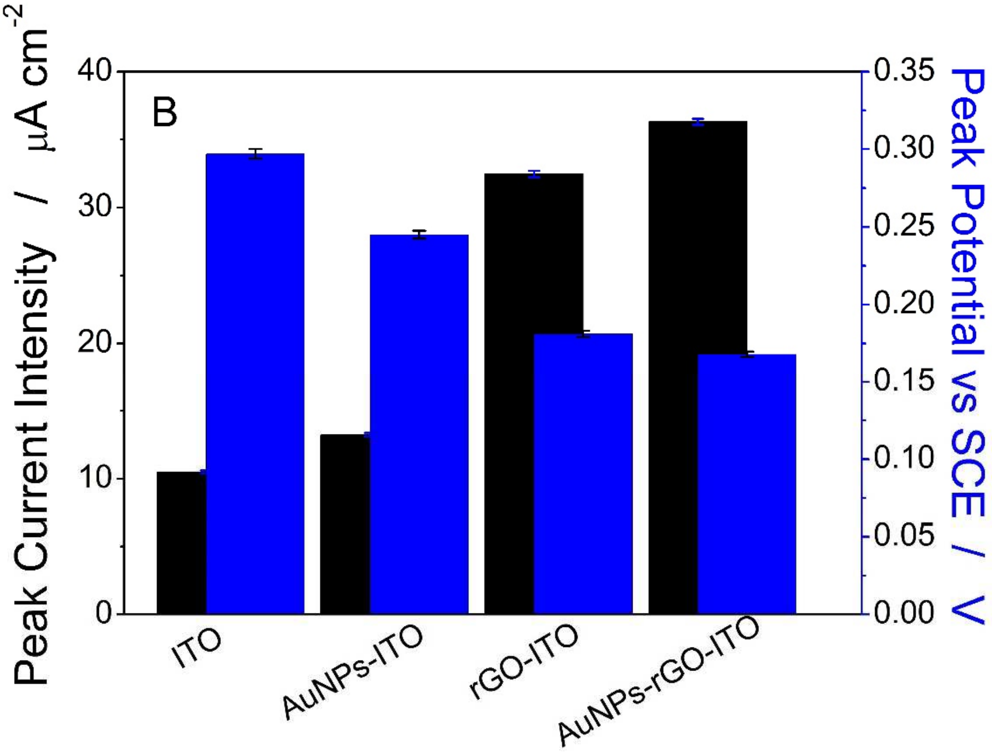
B
Peak Current Intensity / μA cm^{-2}
Peak Potential vs SCE / V
40
30
20
10
0
0.35
0.30
0.25
0.20
0.15
0.10
0.05
0.00
ITO
AuNPs-ITO
rGO-ITO
AuNPs-rGO-ITO

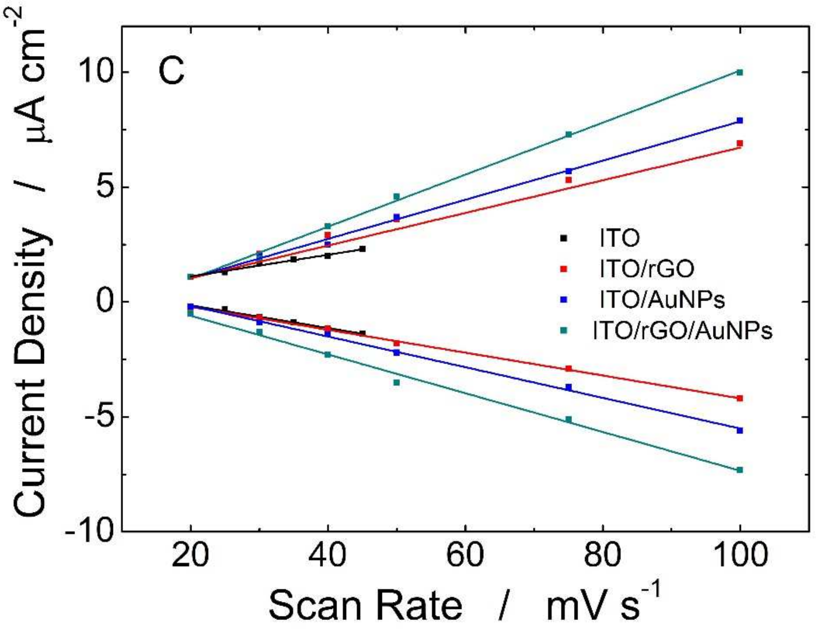

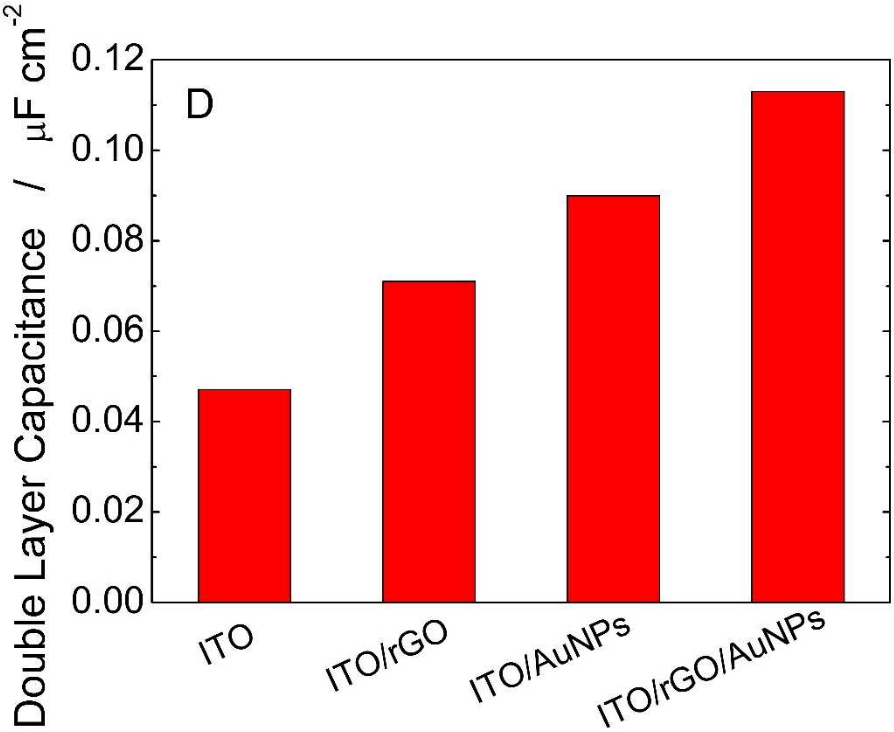

Figure 2 Detection of 25 μM of DA using the progressively modified ITO substrate: (A) SWV curves; (B) Peak current density (black) and peak potential (blue); (C) Anodic and cathodic current density plotted as a function of scan rate; (D) Double layer capacitance. Each experiment carried out 3 times

The same set of electrodes were also tested by CV at different scan rates in order to evaluate the specific capacitance by the double layer capacitance method [63]. The specific capacitance is directly proportional to the real electrode surface and allows the comparison of the different electrode modifications. The measured values of the anodic and cathodic current densities *vs* scan rate are showed in Figure 2C. In the measured scan rate range, a linear behaviour for the all type of electrodes were found. From the slope of these curves the average C_{dl} was calculated and reported in Figure 2D. As expected, the C_{dl} of modified electrodes is at least 2-4 times higher than unmodified ITO-PET. Thus, the modified electrodes have a very high real surface area due to the nanostructured morphology of both Au NPs and rGO. The higher C_{dl} was calculated for the AuNPs-rGO-ITO electrode and thus for this electrode the highest electroactivity is aspect, as confirmed also by the result reported in Figure 2B.

To obtain the best performance, the electrodeposition process of the working electrodes was optimized, in terms of metal precursors and GO concentration, deposition time and potential, using the peak height of 25 µM of DA in the SWV curves as the readout parameter. To study the effect of each investigated parameter, 3 different electrodes with almost identical features, obtained in identical deposition conditions, were used. Each electrode was tested both in the blank solution (PBS) and in the presence of DA. For each parameter, in order to maximize the performance of the sensor, the value corresponding to the highest peak current density in the SWV curves was selected.

Figure 3 shows the effect of (a) applied deposition potential, (b) gold precursor concentration, (c) GO concentration, and (d) deposition time on the peak of 25 µM of DA (see also Figure S6).

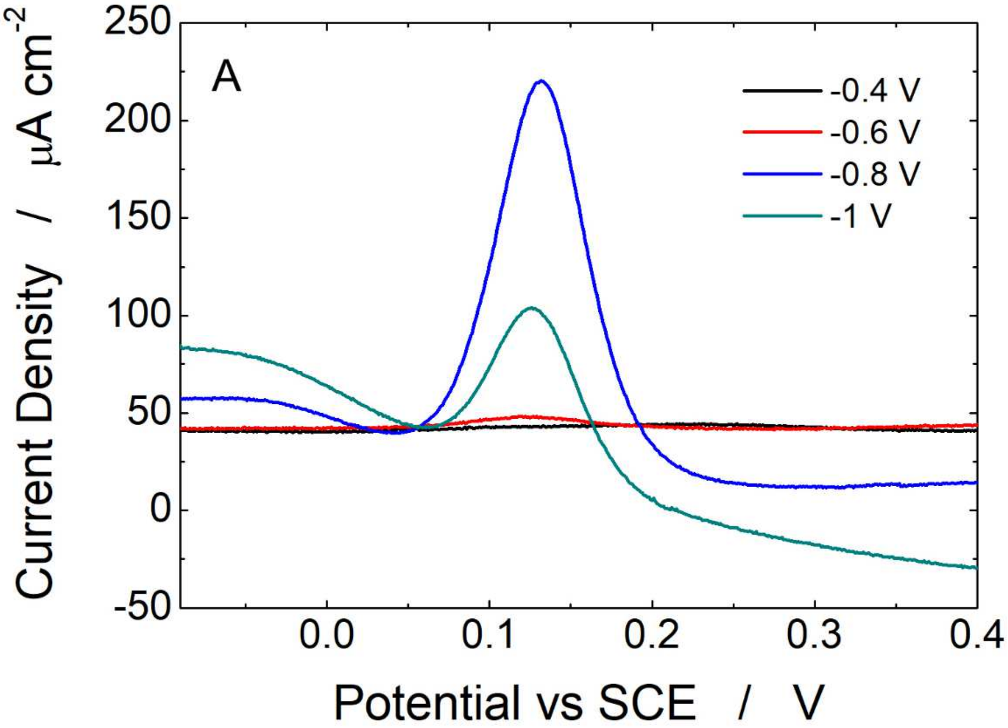
A
-0.4 V
-0.6 V
-0.8 V
-1 V
Current Density / μA cm^{-2}
250
200
150
100
50
0
-50
0.0
0.1
0.2
0.3
0.4
Potential vs SCE / V

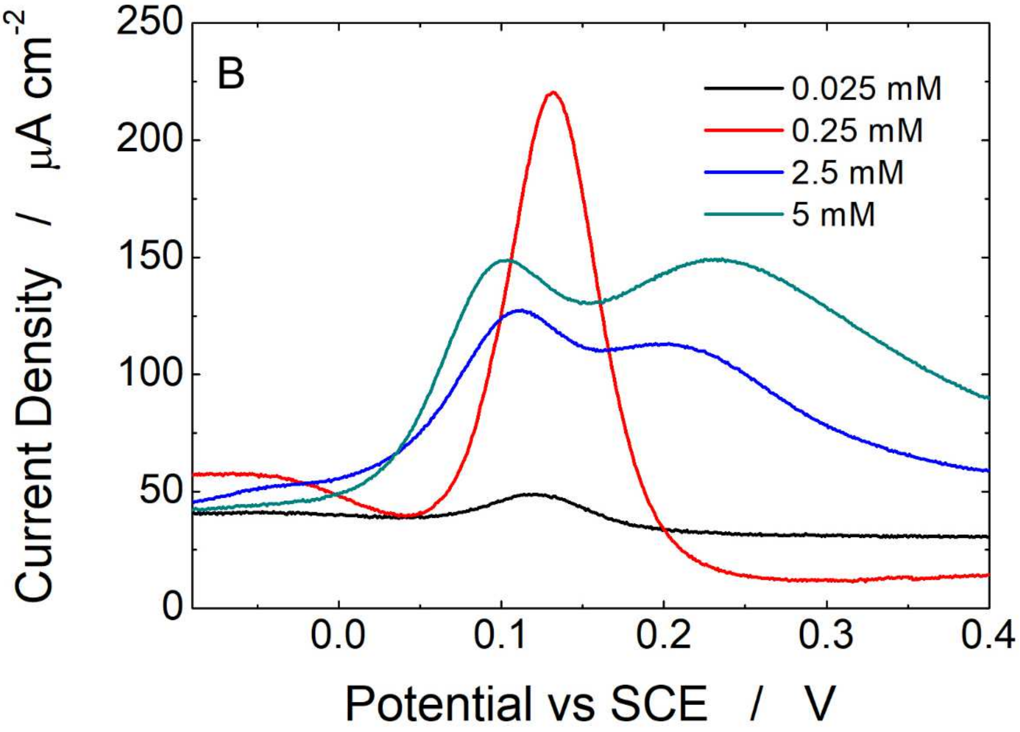
B
0.025 mM
0.25 mM
2.5 mM
5 mM
Current Density / μA cm-2
250
200
150
100
50
0
0.0
0.1
0.2
0.3
0.4
Potential vs SCE / V

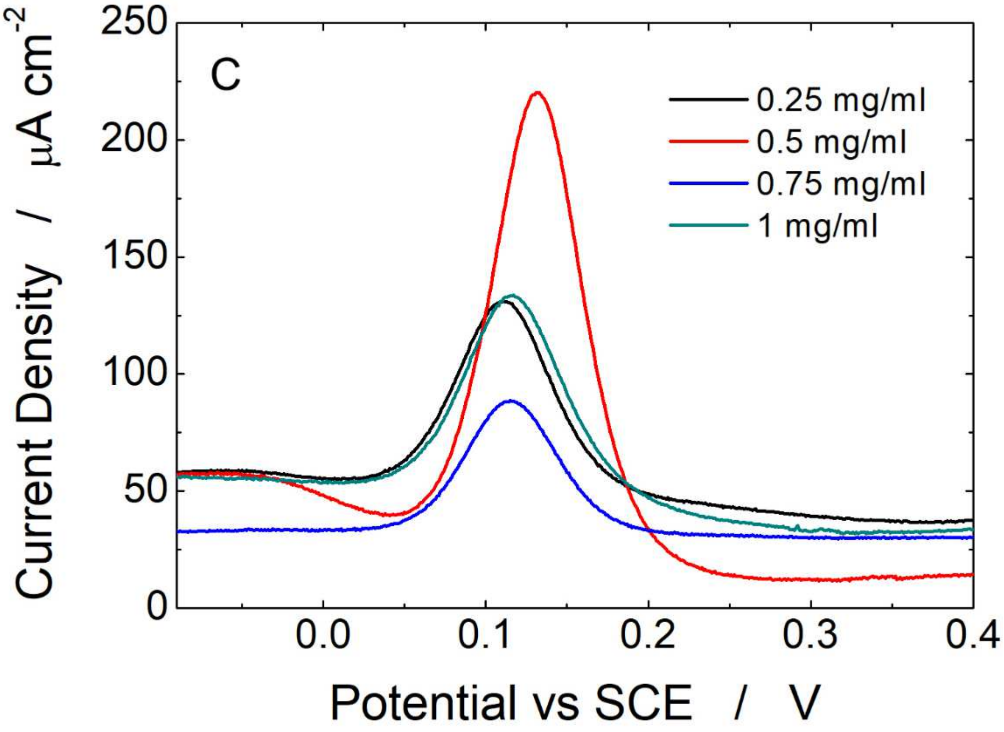
C
0.25 mg/ml
0.5 mg/ml
0.75 mg/ml
1 mg/ml
Current Density / μA cm-2
250
200
150
100
50
0
0.0
0.1
0.2
0.3
0.4
Potential vs SCE / V

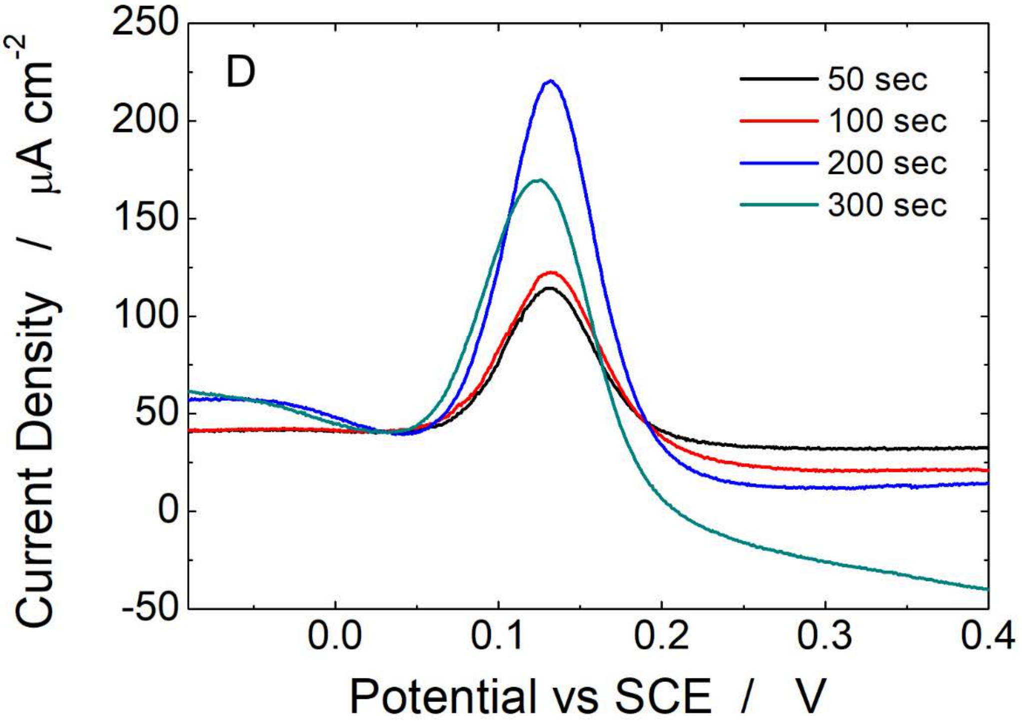

Figure 3. SWV curves showing the effect on the detection peak of 25 µM of DA of (A) applied deposition potential, (B) gold precursor concentration, (C) GO concentration, and (D) deposition time.

Figure 3A clearly shows that for a potential lower than -0.6 V vs SCE the deposition of GO and Au-NPs does not occur. In fact, the peak intensity of DA detection is almost the same of the bare ITO (Figure 2), thus suggesting that no modification of the electrode surface has occurred. This result is in agreement with data previously reported in the literature [40,65,66]. In particular, for rGO it was demonstrated that its reduction starts at a potential of about -0.64V/SCE [66]. When the potential increases catholically up to -0.8 V, the peak current increases, due to the increase of electrochemical active surface area, and then it drops at -1 V. This is probably due to H_2 evolution that acts as secondary reaction, decreasing the efficiency of the deposition of rGO and AuNPs [67]. Thus, the best potential value for the co-deposition of rGO and AuNPS is -0.8 V that assures both the correct loading of substrate and the negligible interference of H_2 evolution. Similar conclusions are also reached using chronoamperometry as detection technique [68]. At -0.8 V vs SCE, the effect of GO and Au precursor concentration was studied and the results are reported in Figure 3B and C, respectively. For increasing gold precursor concentration, from 0.025 to 0.25 mM (Figure 3B), an increase on the peak current intensity (at about 0.15 V vs. SCE) more than 300 % was observed that is attributed to the increase on loading of deposited AuNPS [40]. At higher concentrations of gold precursor, > 0.25 mM, a decrease of the peak current intensity was found, probably due to the morphology of deposited NPs. In fact, with the increase of gold precursor concentration from µM up to mM, the driving force for gold deposition increases and thus the density of deposited NPs. In these conditions, the deposition becomes non-uniform and clusters of NPs are formed due to the coalescence phenomena of nearby nanoparticles. This leads to a decrease of the electroactive surface area of the electrode that justifies the lower measured peak current. This hypothesis was confirmed by FESEM analysis of these type of samples (Figure S7) characterized by the presence of cluster of particles of about 0.1/0.2 µm, higher compared to the NPs visible in Figure 4B, where a high-magnification FESEM image of the optimized electrode is reported. For high concentration of gold precursor, and consequently high amounts of deposited Au on the electrode surface, a second peak at about 0.25 V vs. SCE appears, that is attributable to Au oxidation. In the case of GO concentration, Figure 3C, the best compromise was achieved for a GO content of 0.5 mg/mL where a maximum peak current for DA detection was observed. Under these conditions, a high electrochemical active surface area was obtained, which ensured a good electrocatalytic behaviour. For higher concentrations, the excessive loading of GO, resulted in a consequent decrease of surface area, negatively affecting the electrode performance, as also reported in [69]. The effect of deposition time, Figure 3D, was investigated at -0.8V vs SCE with 0.5 mg/mL of GO and 0.25 mM of gold precursor. It was found that the best value for this parameter was 200 sec, which corresponds to a maximum observed peak current intensity. Once again, for low deposition time (below 200 sec) the loading of GO and AuNPs is low and thus low is their electrocatalytic effect. For higher values, the excessive load of rGO and AuNPs causes the formation of a more uniform and compact electrode surface characterized by a low electroactive surface area. A similar behaviour was obtained by carrying out the same detailed series of experiments for electrodes based on rGO and PtNPs. In Table 1, a summary of the optimized values of each parameter for both types of electrodes is presented.

Table 1. Optimized values of electrodeposition parameters to obtain AuNPs-rGO-ITO based sensors

	AuNPs-rGO-ITO	***PtNPs-rGO-ITO***
Media	ABS	ABS
Deposition Potential	-0.8 V vs SCE	-0.8 V vs SCE
GO concentration	0.5 mg/mL	0.5 mg/mL
Metal precursor concentration	0.25 mM	0.25 mM
Deposition time	200 sec	300 sec

The optimized electrodes were characterized by FESEM, EDS, XRD, Raman spectroscopy and XPS. Figure 4 and 5 show the results of this characterization in the case of optimized gold-based electrodes. Similar results were obtained with the Pt-based electrode and results are shown in Figure S8 of the supplementary material. The FESEM images of Figures 4A and 4B show that the gold nanoparticle deposition was well dispersed. NPs had a mean diameter of 25.6 ±3 .8 nm. Also, the rGO sheets are evident and appear well attached into the electrode surface. The wrinkle-like sheet morphology is typical of rGO and provides a high surface area which enables efficient electrochemical reactions [70]. In the EDS spectrum presented in Figure 4C, the presence of gold peak suggests the effective deposition of the Au NPs. The peaks of indium arise from the underlying ITO deposited on PET substrate while C and O are attributed mainly from the PET and also from the electrodeposited rGO.

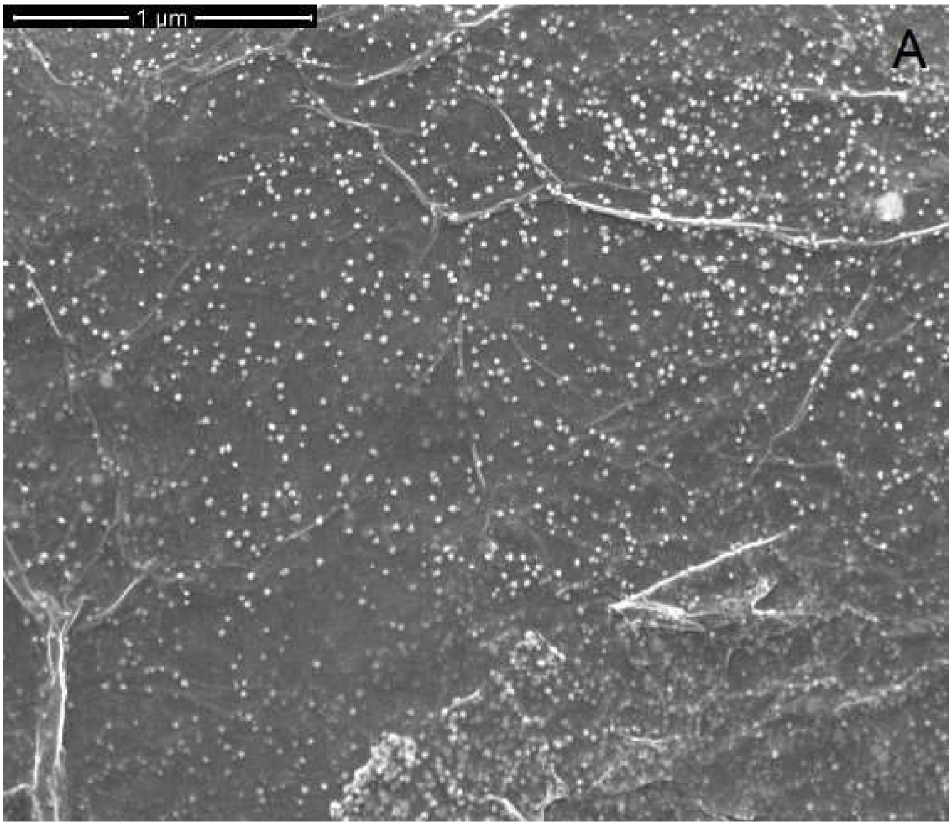
1 µm
A

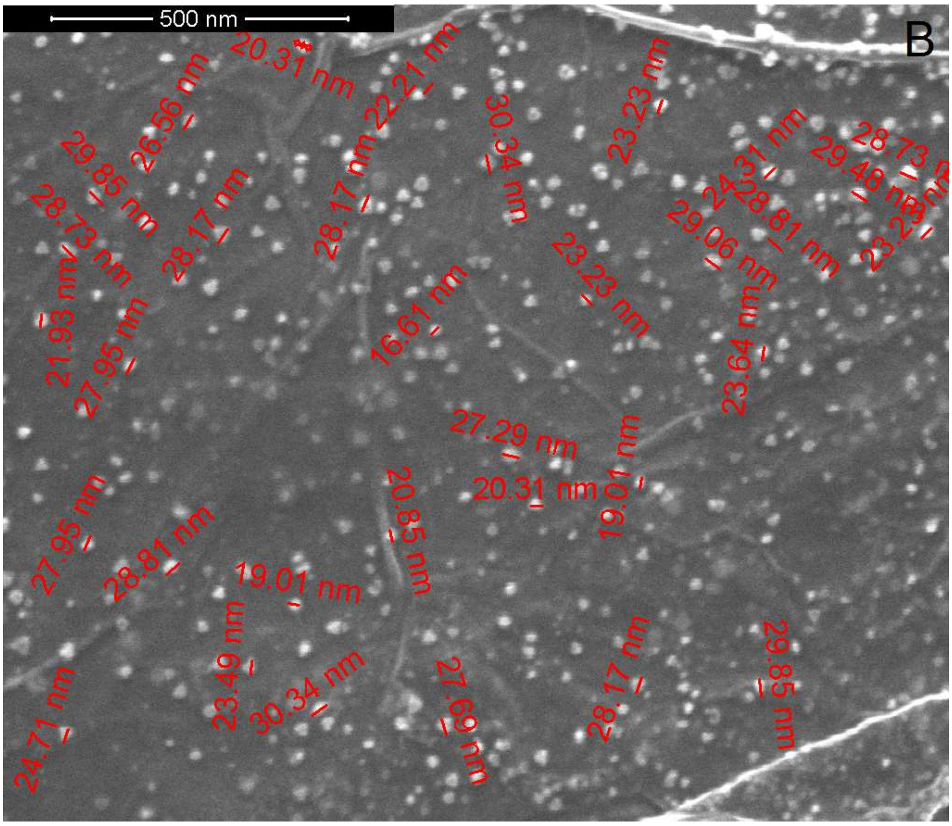
500 nm
B
20.31 nm
26.56 nm
22.21 nm
30.34 nm
23.23 nm
29.85 nm
28.17 nm
28.73 nm
28.17 nm
24.31 nm
29.48 nm
28.73 nm
28.81 nm
29.06 nm
23.23 nm
21.93 nm
27.95 nm
16.61 nm
23.64 nm
27.29 nm
20.31 nm
19.01 nm
20.85 nm
27.95 nm
28.81 nm
19.01 nm
23.49 nm
30.34 nm
27.69 nm
28.17 nm
29.85 nm
24.71 nm

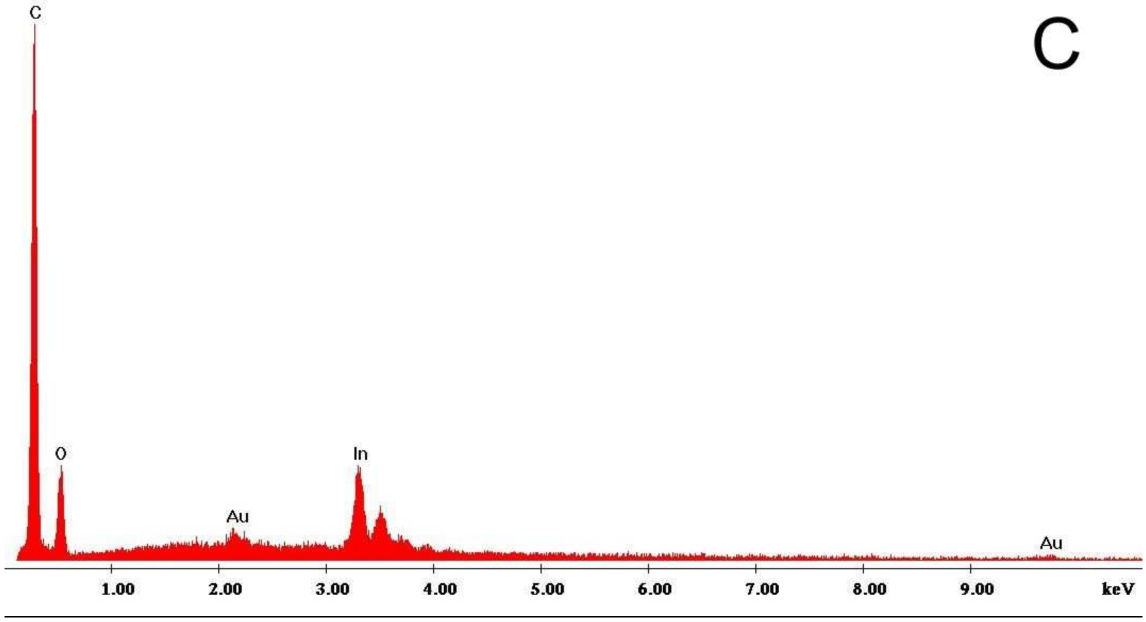

Figure 4. (A-B) FESEM images and (C) EDS spectrum of rGO-Au-NPs/ITO based sensors.

Figure 5A shows the XRD pattern of the as prepared electrode. The broad peak centered at about 2θ = 23.7°, corresponding to the (002) diffraction plane, confirms the deposition of reduced GO as reported in [71]. Appling the Bragg's equation [72] to this reflection, the distance between rGO layers was calculated at a value of ~ 0.38 nm, that agree with results reported in [73]. The peaks at 2θ about to 38° and 44° are attributed to deposition of polycrystalline gold with main orientation along the (111) diffraction plane. The main diffraction peak of gold, located a t 38.2°, is quite broad suggesting the formation of a deposit with a small grain size. To verify this, the Sherrer's equation [72] was used to calculate the mean grain size of Au NPs. In particular, on the basis of the width at half height of the main diffraction peak of gold, a mean value of about 20.30 ± 0.2 nm was calculated, consistent with FESEM measurements.

The Raman spectrum shown in Figure 5B is further confirmation of the presence of rGO. In fact, the main bands at about 1343 cm^{-1} and 1588 cm^{-1} are present and attributed to D and G band, respectively, as reported in [74]. The main bands of rGO are about in correspondence of Raman modes of ITO-PET substrate (black curve), thus a convolution by Gaussian fitting was necessary to better evaluate the intensity of these bands. While in GO the intensity of the two bands is comparable (red curve), in the AuNPs-rGO-ITO samples the intensity of D band is higher (about 16%) then G. This is attributable to the presence of rGO [75], and is due to the increase of structural disorder because the GO reduction.

Electrodes were further characterized by XPS and the spectra are reported in Figure 5C and D. In the case of Au 4f, see Figure 5C, two contributions were found by curve-fitting analysis of the two spin-orbit components (Au $4f_{7/2}$ and Au $4f_{5/2}$) of the Au4f. The first Au$4f_{7/2}$ component at BE of 83.95 eV is associated to Au^0, while the second Au$4f_{7/2}$ component at BE of 84.56 eV is assigned to Au^+. These results are expected for Au NPs and are in agreement with those previously reported in [76]. The Au^+ is about 8% of the total gold. Figure 5D shows the XPS spectrum of C 1s. In the deconvoluted spectrum the presence of C=C (284.96 eV, 73.92%), C-O-C (286.57 eV, 18.82%), and O-C=O (288.62 eV, 7.27%) bonds was identified. The high intensity of C=C and the absence of -COOH peak (289.5 eV) confirm the reduction of GO during the electrodeposition process [77].

In conclusion all characterization techniques indicate the presence of AuNPs and rGO on the surface of electrode.

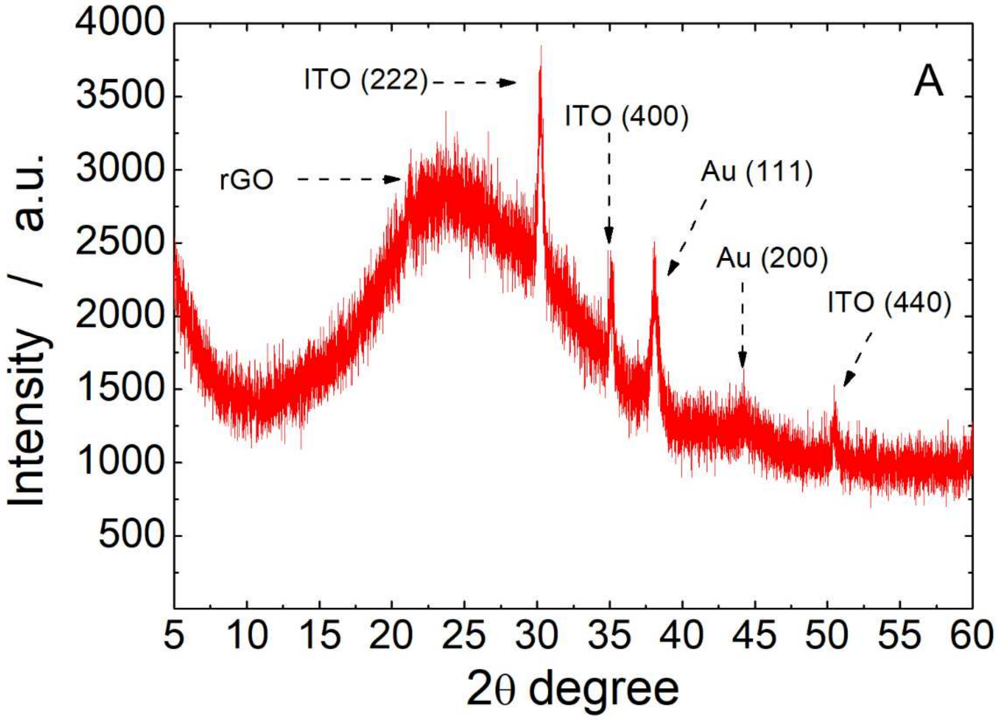
A
Intensity / a.u.
2θ degree
rGO
ITO (222)
ITO (400)
Au (111)
Au (200)
ITO (440)
4000
3500
3000
2500
2000
1500
1000
500
5
10
15
20
25
30
35
40
45
50
55
60

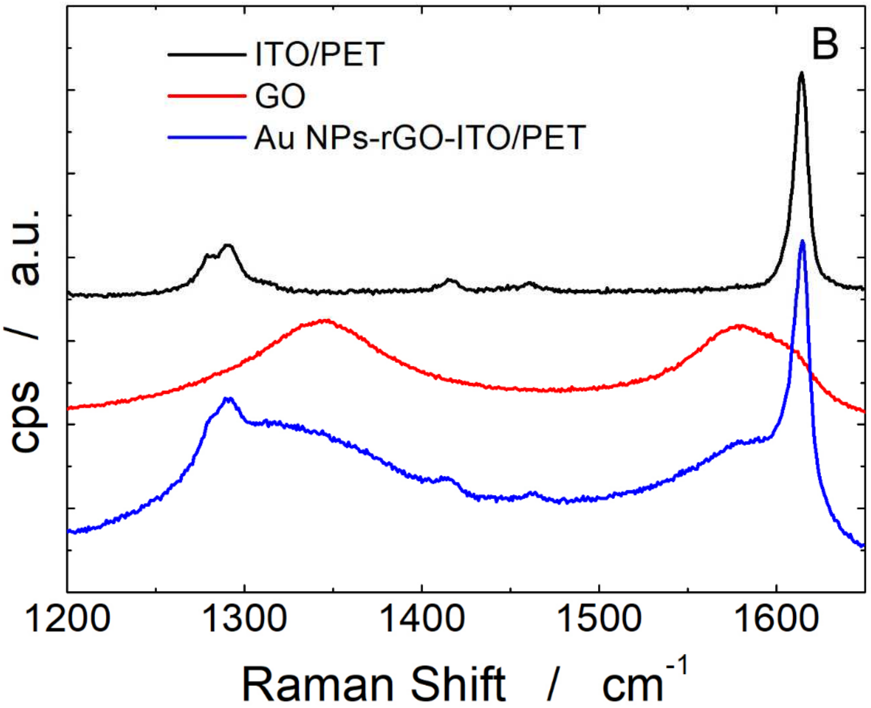
B
ITO/PET
GO
Au NPs-rGO-ITO/PET
cps / a.u.
Raman Shift / cm-1
1200
1300
1400
1500
1600

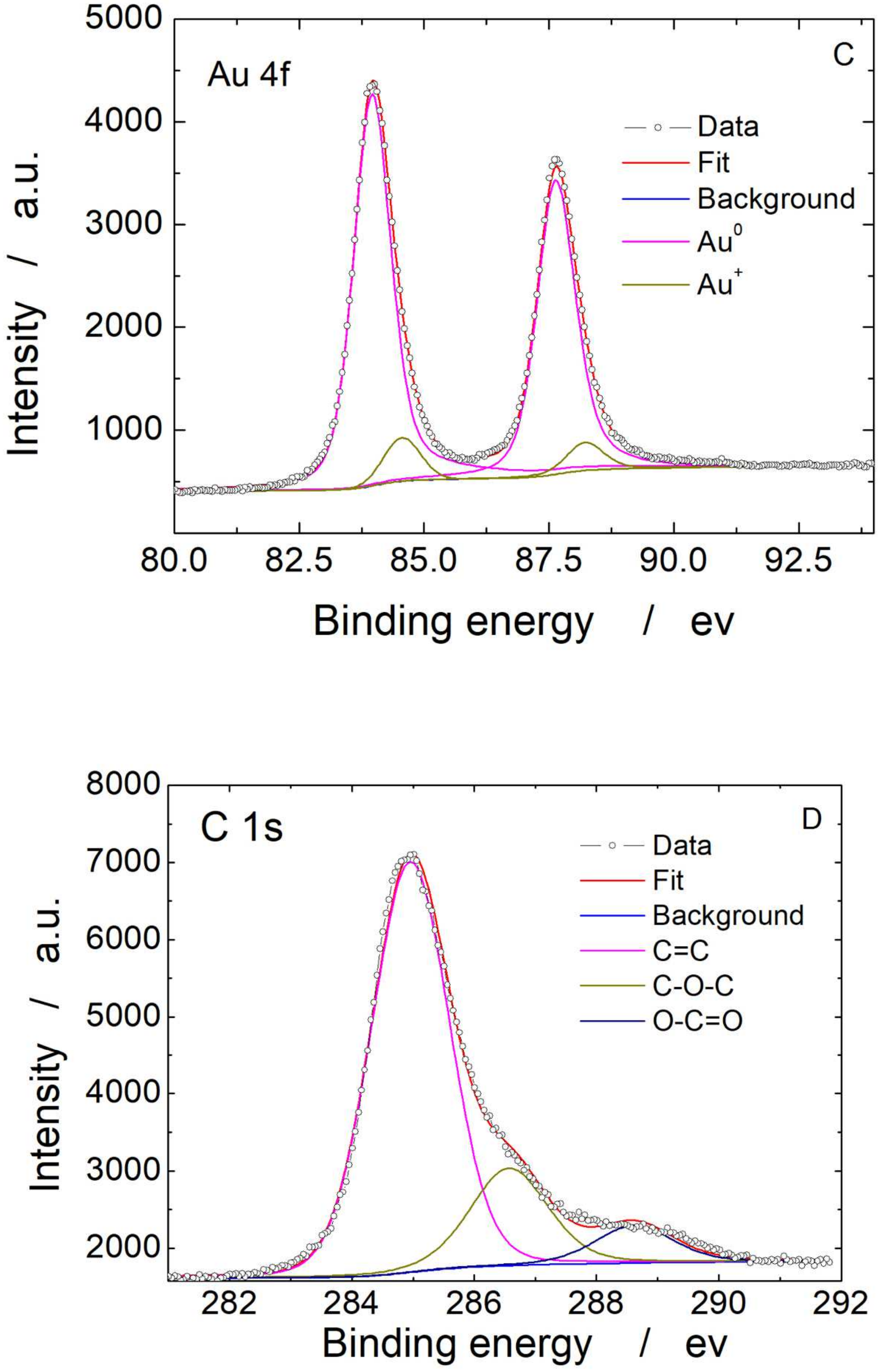

Figure 5. (A) XRD pattern, (B) RAMAN spectrum of rGO-Au-NPs/ITO based sensors and (C and D) XPS spectra ((C) Au 4f and (D) C 1s)). In Figure B, for comparison, also the spectra of bare ITO and GO powder was reported.

3.2 Sensor Performance

The effect of the pH of solution on DA detection was investigated and the results were reported in Figure 6. According to the Minta ed al [78], with the increase of pH, in the range 5-8, the peak potential, Figure 6A, shifts towards lower values with a linear dependence having a slope of about -44 mV/pH unit. The current density maximum is reached at pH 7, Figure 6B. Despite this result, the electrochemical characterization of the sensors was performed at pH 7.4 as this is the value typically employed by other groups and therefore allows back comparison of our sensors with the literature.

Sensor calibration was carried out in PBS while varying the DA concentration range from 1 to 500 μM, using both AuNPs-rGO-ITO and PtNPs-rGO-ITO as working electrodes. For AuNPs-rGO-ITO, the results are shown in Figure 7 A-C, while for PtNPs-rGO-ITO the results are reported in Figure 6D and in Figure S9.

Concerning AuNPs-rGO-ITO based sensors, Figure 7A shows the SWV curves for different DA concentrations. These experiments were repeated 3 times using electrodes with almost identical features and the mean peak current intensity value with relative error bars (both reproducibility and repeatability) are reported in Figure 7B. From Figure 7A, it was observed that the peak potential value of DA detection remains unchanged with increasing DA concentration. The DA peak appears at 0.1 μM and its intensity linearly increases up to 20 μM. At higher concentrations (Figure 7B), the peak intensity still has a linear dependence from DA concentration but with a lower sensitivity (1.76 $\mu A\ \mu M^{-1}\ cm^{-2}$). This is a common behaviour of electrochemical sensors [35,79]. The dopamine sensitivity calculated from the slope was shown to be 6.02 $\mu A\ \mu M^{-1}\ cm^{-2}$ (Figure 7C). The estimated LOD is 75 nM calculated using a signal to noise ratio of 3.3.

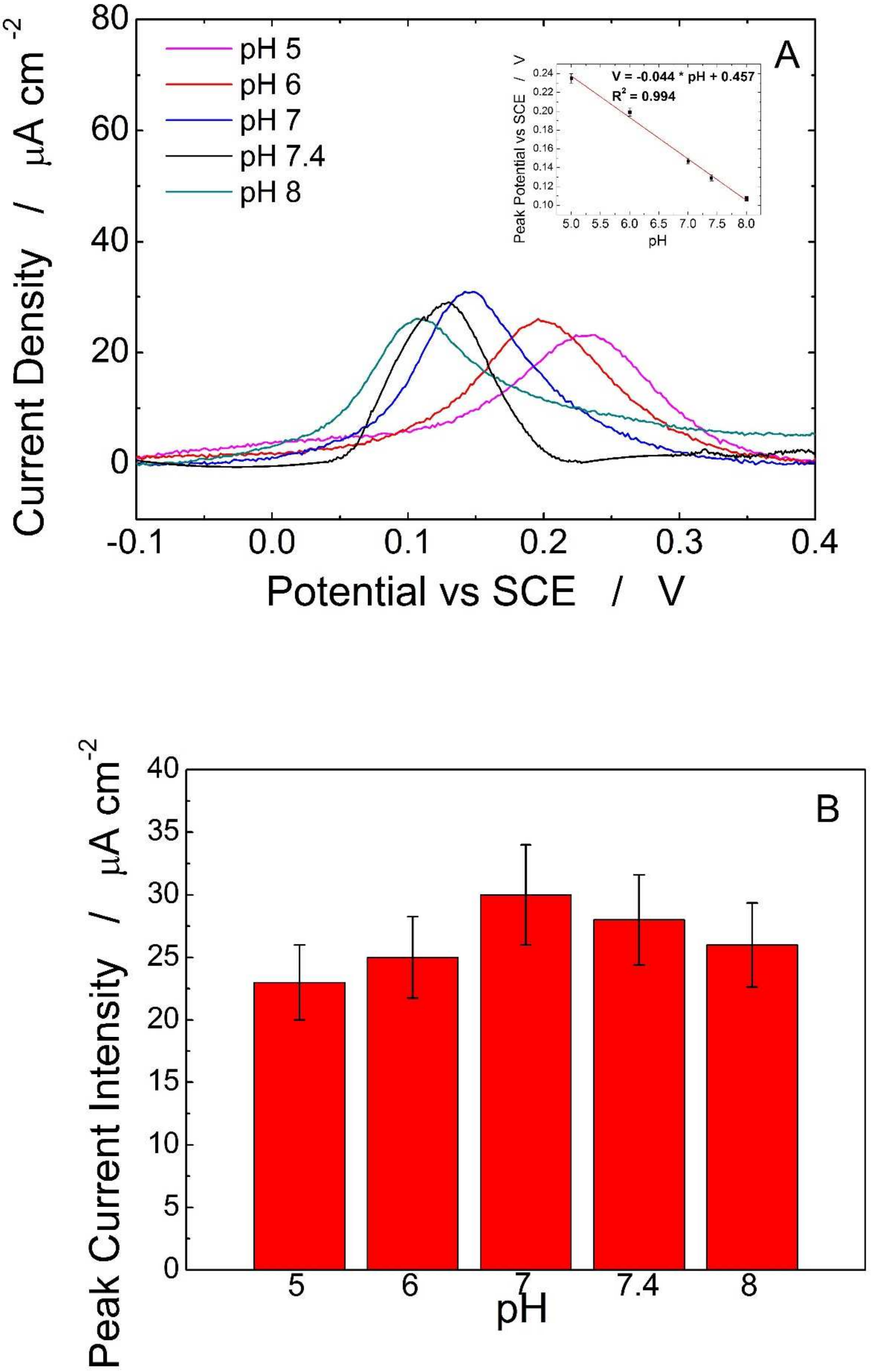

Figure 6. Effect of the solution pH on DA detection: A) SWV curves and B) peak current density. Each experiment carried out 3 times

Considering PtNPs-rGO-ITO based sensors, an interesting behaviour was observed and present in Figure 7D. In fact, for both type of sensors a similar LOD was reached, but in the case of PtNPs-rGO-ITO a higher sensitivity but with a narrower linear range was measured (Figure S10). In particular, the DA detection peak started to increase linearly from 0.1 to 10 µM DA with a sensitivity of 7.19 µA μM^{-1} cm^{-2} and an estimated LOD of 62 nM. The high sensitivity clearly shows that PtNPs possess higher catalytic activity towards DA oxidation in comparison to Au [80]. For both electrodes the LOD values are lower than the expected DA concentration in real samples, for example in the case of urine is about 0.6 µM, thereby showing their suitability for this application [81]. The excellent performance of the sensor can be attributed mainly to the very good electrocatalytic properties of rGO towards the DA detection [27], and also to the nanostructured morphology of the sensor surface. In fact, a nanostructured surface ensures a high electrochemically active surface area, characterized by a large number of active sites where the DA oxidation can take place.

As stated before, one of the main issues in the electrochemical detection of DA in real complex sample matrices, is the interference from other species, especially ascorbic (AA) and uric acids (UA). For both species, the problem for DA detection is related to the similarity of their redox potentials (0 V and 0.3 V vs SCE respectively) which are close to DA ~0.12 V. As these compounds are always present in body fluids in a concentration range of about 100-1000 times higher than DA (present in the sub µM range) the peaks of AA and UA can significantly overlap with, and swamp the detection peak of DA [56,57]. To this end, a characterisation study was undertaken for the detection of DA in the presence of AA and UA. Figure 8A-B shows the SWV, using AuNPs-rGO-ITO as working electrode, in presence of different amounts of DA and increasing concentrations of UA and AA.

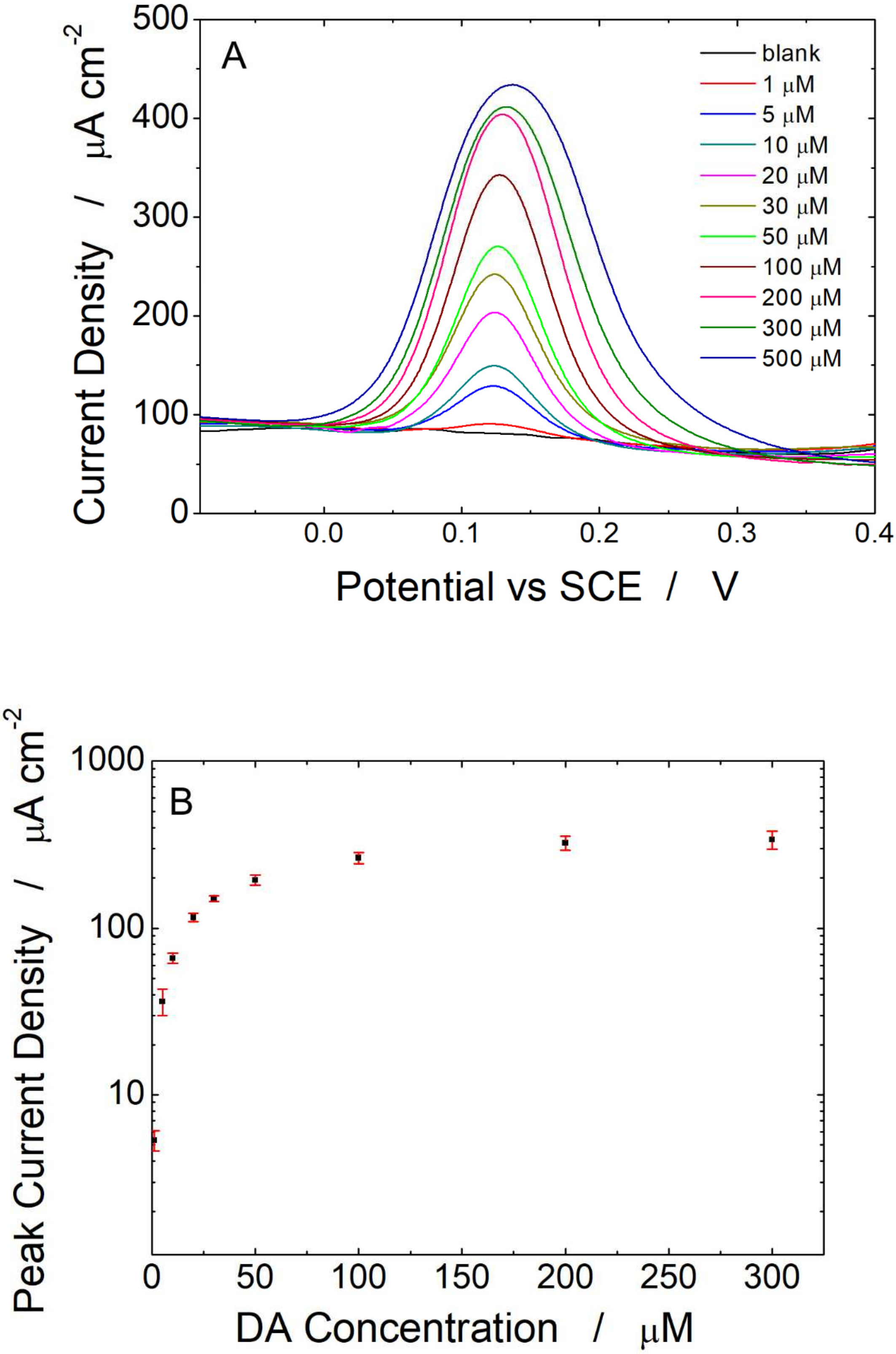

A
Current Density / μA cm^{-2}
Potential vs SCE / V
0
100
200
300
400
500
0.0
0.1
0.2
0.3
0.4
blank
1 μM
5 μM
10 μM
20 μM
30 μM
50 μM
100 μM
200 μM
300 μM
500 μM
B
Peak Current Density / μA cm^{-2}
DA Concentration / μM
10
100
1000
0
50
100
150
200
250
300

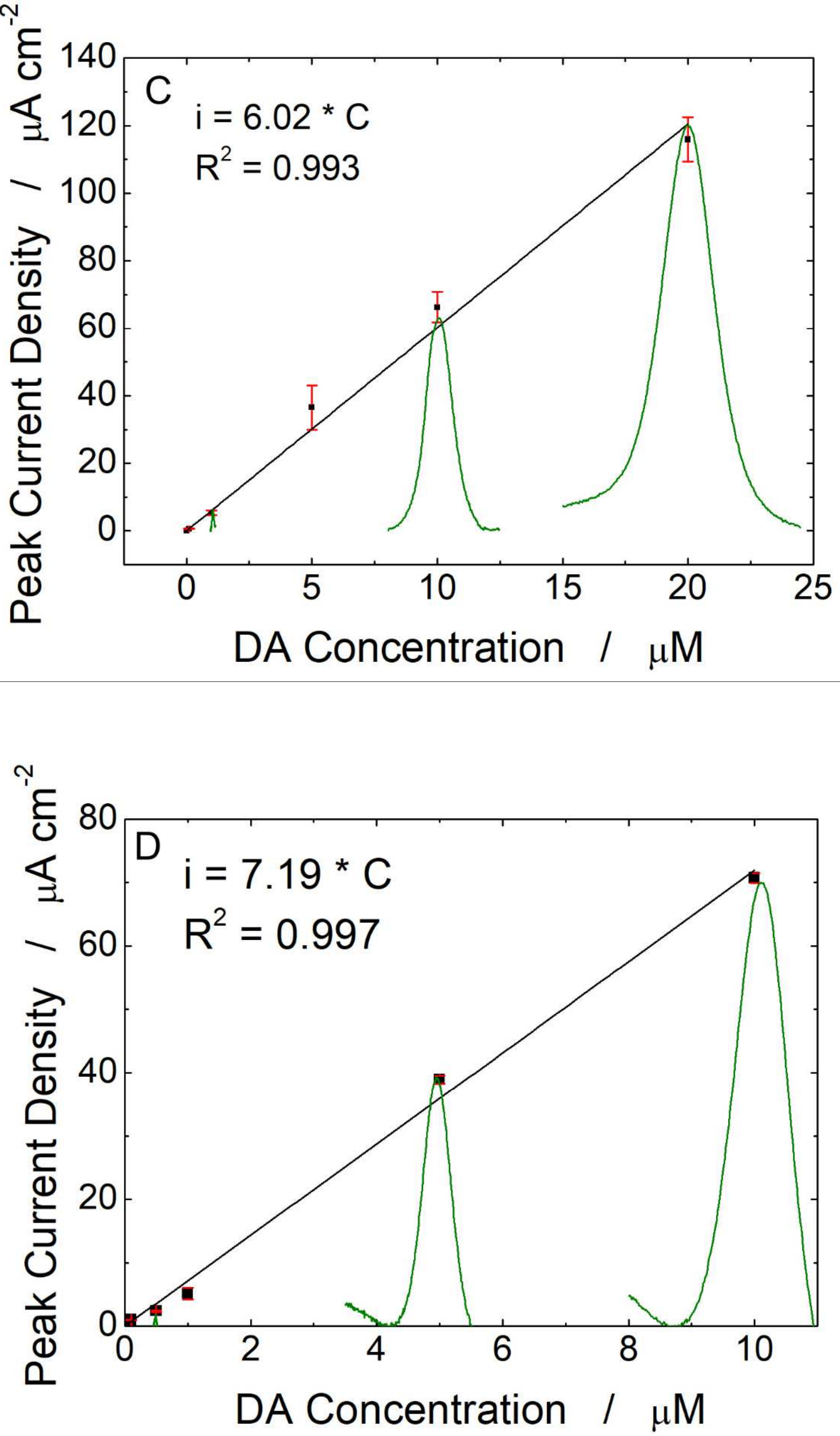

Figure 7. (A) SWV curves, (B) peak current density vs DA concentration and (C) relative calibration line using AuNPs-rGO-ITO based sensors. (D) Calibration line using PtNPs-rGO-ITO based sensors. Each experiment was carried out 5 times

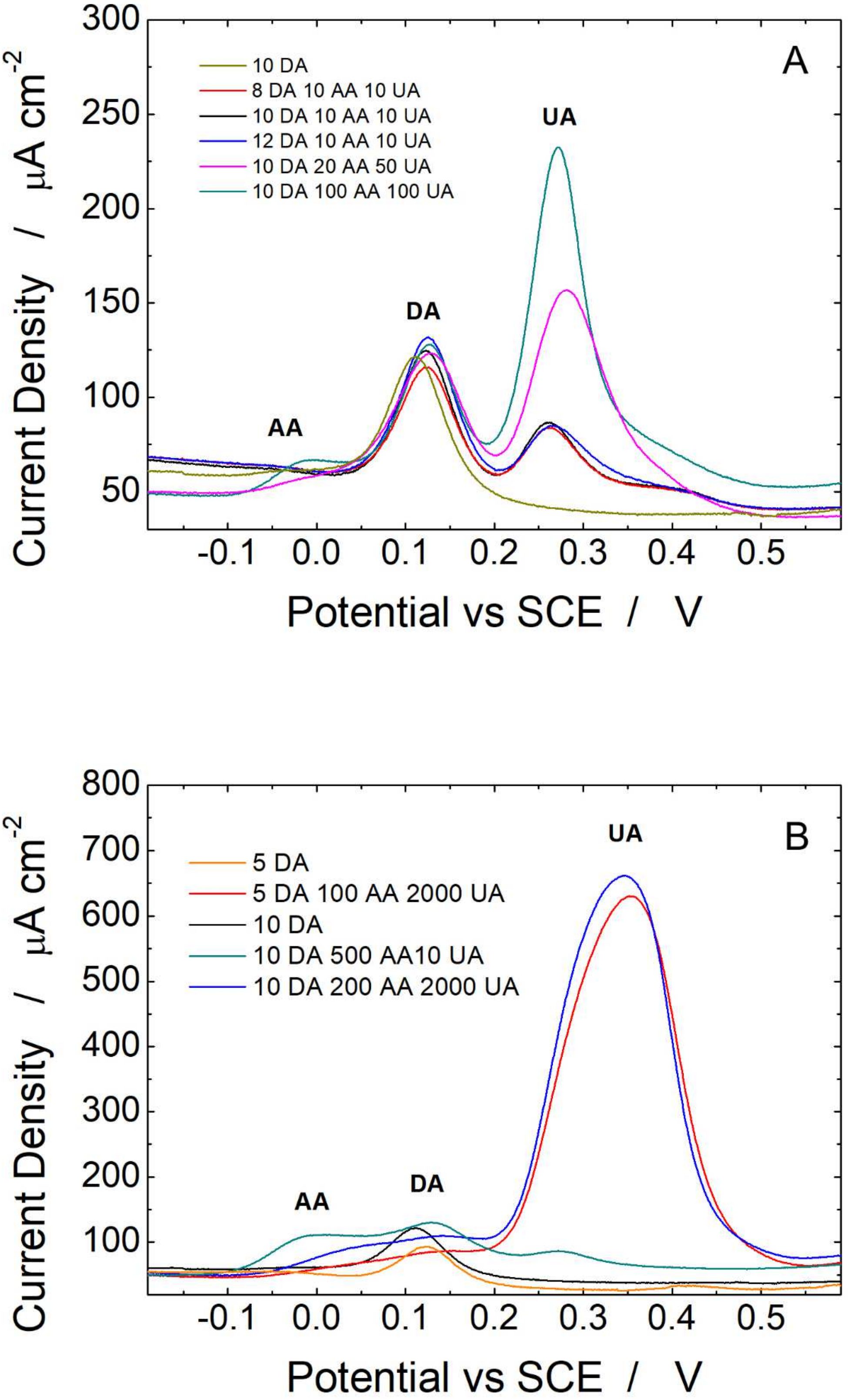

Figure 8. Effect of different concentration of ascorbic acid (AA) and uric acid (UA) on the detection of DA.

At low AA and UA concentrations, Figure 8A, even with a ratio 1/10 of DA/AA and DA/UA the DA detection peak is present and, more important, its intensity is consistent with the results of the calibration line (Figure 7C). These results suggest the ability of the electrode to simultaneously detect DA, AA and UA (the mechanism of electrochemical oxidation of UA and AA was reported in Figure S11). Figure 8B shows the peak of 5 and 10 μM DA in presence of higher concentration of AA (0.5 mM) and UA (2 mM). Interestingly, high concentration of AA does not lead to any interference effects (see green and black curve) in the detection of DA. As reported in the literature, this behaviour is attributed to the electrostatic repulsion between GO and AA that causes the suppression of AA oxidation [27]. Concerning UA, its presence in the concentration of 2 mM (this value is plausible in real samples of urine) led to a loss in sensor detection of about 8%. Thus, from the interference study, it can be concluded that high UA concentrations may lead to a slight interference on DA detection, while AA does not have any effect.

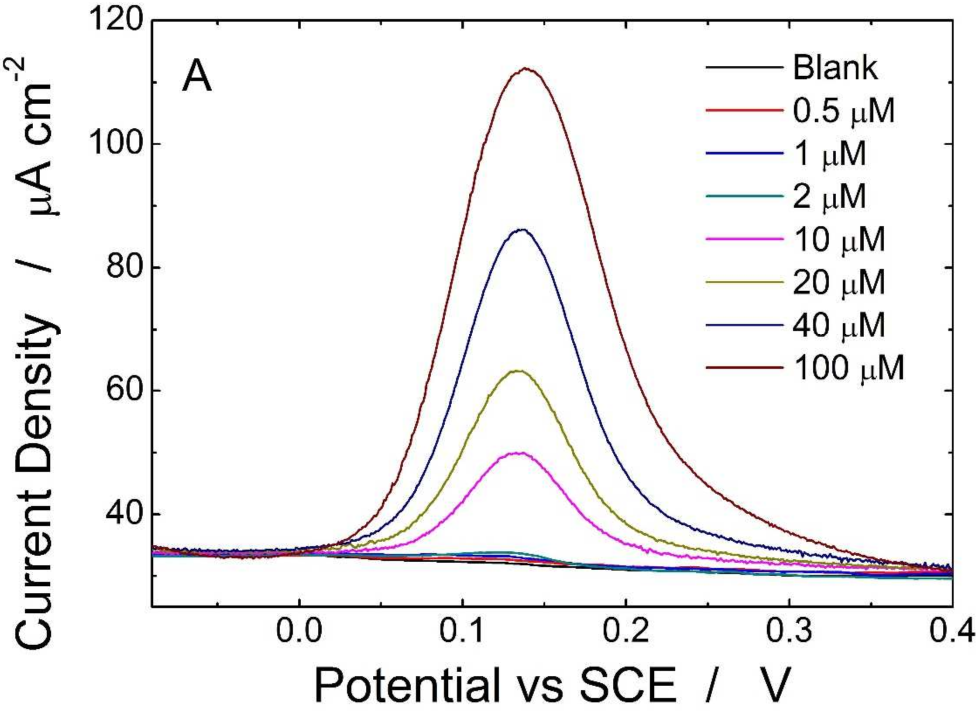

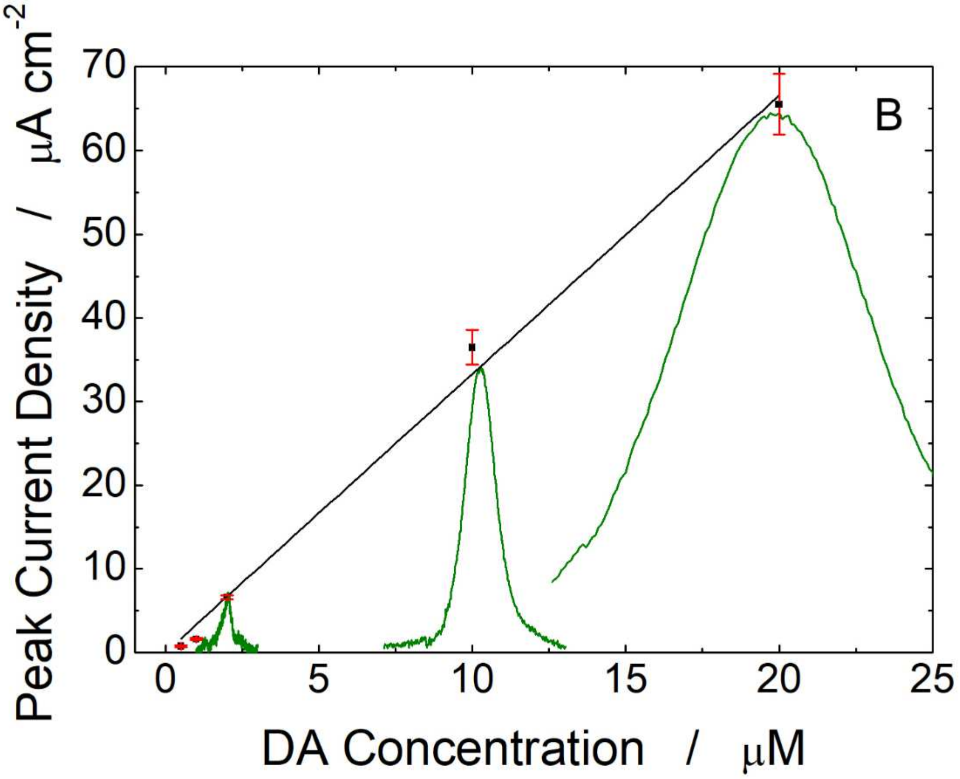

Figure 9. (A) SWV curves for the detection of different DA concentration using AuNPs-rGO-ITO based sensors in synthetic urine; (B) relative calibration line. Each experiment carried out 5 times

In order to simulate the operation of the sensor in a real sample, DA detection has been carried out in commercially available synthetic urine Synthetic urine has all the properties and characteristics of real urine therefore it can be used as a control solution during assay development work. Using the optimized electrode based on Au NPs, a calibration line was obtained in synthetic urine and the results presented in Figure 9 (see also Figure S12). The results show that the determination of DA in urine matrix is still possible with good sensitivity. Particularly, a linear range from 0.1 to 20 μM was obtained, similar to PBS, but with a lower sensitivity of 3.365 μA μM^{-1} cm^{-2}. This decrease in sensitivity could be due both to the presence of different chemical species present in the urine matrix (that may be cause fouling or interference problems) and/or to the different pH (>8) of the synthetic urine. Considering that the pH plays an important role on the DA determination, as shown in Figure 5 and in the literature [35,49], we hypothesise that the different pH is the main cause.

In order to verify the flexibility of the sensor, the detection of DA was performed after different deformation cycles of the sensors. In particular, the electrode was bent, stretched and totally twisted (Figure S13) for five times and then tested to detect DA. As can be observed in Figure 10, the bent and stretched electrodes have the same behaviour as a pristine sensor, and thus these deformations do not alter the functionality of the sensor. For twisted electrodes, a drastic decrease in peak current is observed, indicating that this type of deformation significantly damages the conductive substrate.

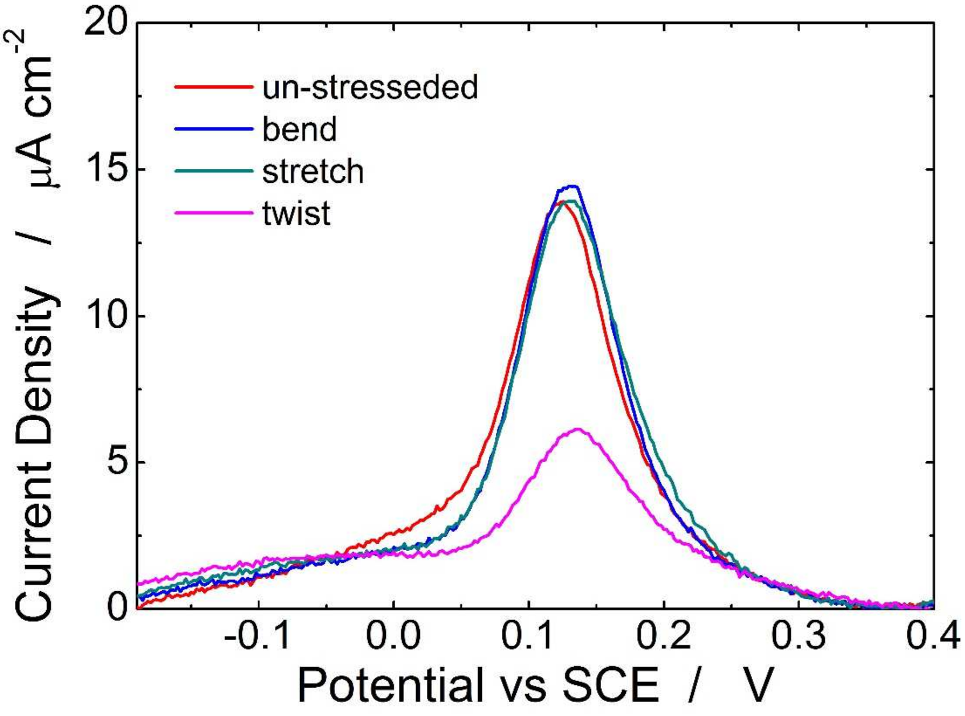

Figure 10. SWV curves for the detection of DA after different deformation of the electrodes

To further validate the sensors, real urine samples were also tested. In particular, the urine was collected for 24 h and tested in an authorized analysis laboratory by HPLC. From HPLC analysis, a concentration of 243.8 μg/24h (see Figure S14) equal to 0.69 μM was determined.

The same urine sample was tested using the AuNPs-rGO-ITO electrode. To perform the electrochemical detection, the urine samples were diluted (50% in volume) with PBS (to reach a pH similar to synthetic urine used to obtain the calibration line) and DA was detected using the SWV technique discussed previously. Three different electrodes employed, and using the calibration line developed in synthetic urine (see Figure 9B), a concentration of 0.65 ± 0.042 μM was determined. It is important to highlight that, in real urine, three different cathodic peaks were found relative to DA, UA and AA oxidation. Despite the presence of UA and AA the sensor is able to detect DA with a precision comparable to the standard technique (recovery of ~ 94%), demonstrating again the negligible interference of these compounds on DA detection. Thus, these results clearly demonstrate the possibility of using the as developed sensor to quantify DA in urine samples.

The sensitivity of the developed sensors is excellent compared to other electrochemical sensors for DA detection [11] (see also Table 2, where a comparison between non enzymatic electrochemical sensors for dopamine detection was reported). In fact, just few reports show a sensitivity higher than 1 μA μM^{-1} cm^{-2} while our sensor features a sensitivity of 3.365 μA μM^{-1} cm^{-2} in urine samples. The high sensitivity of the obtained sensors is attributable not only to the presence of very good electrocatalytic material but also to a careful balancing of MtNPs and rGO loading ensuring a high electrochemical active surface area. In particular, the careful loading of the substrate ensures the presence of the correct amount of active material, on which the properties of electrocatalytic activity and selectivity towards DA depend, and at the same time also exhibit a high electrochemically active area and therefore a high presence of active sites for the DA oxidation, to which the sensitivity of the sensor is linked.

All of these features, combined with the very short preparation time (200 sec), the simplicity of the preparation method (co-electrodeposition from aqueous electrolyte containing a very low concentration of the precursors of gold and graphene oxide) and the low fabrication costs (laboratory estimated cost at around € 0.2/sensor), make this sensor easily scalable and therefore applicable on a large-scale application.

Table 2 Comparison between non enzymatic electrochemical sensors for dopamine detection

GCE = Glassy Carbon Electrode, PANI = Polyanylyne, rGO = Reduced Graphene Oxide, SPCE = Screen Printed Carbon Electrode, IL = Ionic Liquid, GME = graphene modified electrode; GrQD = Graphene Quantum Dots, CS = Chitosan, CSF = Carbonized silk fabric, CP = Carbon Paste, MOF = Matal-organic framework, CNT = carbon nanotube, MWCNT = multi-walled carbon nanotube, HBNGH = f 2,2′-[1,7-hepthandiylbis (nitriloethylidyne)]-bis-hydroquinone, PPyox = overoxidized polypyrrole, HCS = hollow carbon sphere, PEDOT = poly(3,4-ethylenedioxythiophene), Gr = graphene, DPV = Different Pulse Voltammetrym, CV = Cyclic voltammetry, CH = Chronoamperometry, TRS = Transitor, AA = Ascorbic Acid, FC = Folic Acid, SE = Serotonyn, AC = Acetomiophene, CYST = Cysteine, GLU = Glucose, UA = Uric Acid, LAC = Lactose, TYR = Tyrosine =PHEN = phenylalanine CA = Citric Acid O-PD = O-phenylenediamine , P-PD = P-phenylenediamine GLY = Glycine, PHA.SA = Pharmaceutical Samples, DA.HYD = Dopamine Hydrochloride, ACOP = Paracetamol, β-CD = β-cyclodextrin, EP= epinephrine, NEP = norepinephrine, NS = Not Shown

*This value was approximately calculated by us.

Sensor Type	Technique	Sensitivity μA μM^{-1} cm^{-2} *Linear range* μM	LOD μM	Interference	Real sample	Ref
GCE/PANI/NiO	DPV	1.1 0.2-2.4	0.0153	AA, SE	PHA.SA	[82]
Polytryptophan-graphene	DPV	2.09* 0.2-100	0.06	K^+, Na^+ , Cl^- , SO_4^{2-} , Ca^{2+}, Zn^{2+}, Mg^{2+} CYST, TYR, PHEN, AA	DA.HYD	[83]
rGO-AuNPs-GCE	CH	3.55 0.14-100	0.137	CA, GLU, $NaNO_3$, Na_2CO_3	NS	[39]
PolyDA-rGO-SnO2-Au NPs	DPV	24.7* 0.008-20	0.005	AA, UA	Urine, Serum	[46]
Polypirrole-rGO-Pd NPs	DPV	0.024* 38-1647	0.056	AA, UA	Serum	[84]
N doped-rGO	DPV	3.2* 1-60	0.1	AA, UA	NS	[85]
SPCE-IL-GrQD	DPV	10.03 0.2-15	0.06	AA, UA	PHA.SA	[86]
Nafion/rGO/CSF	TRS	1.065 0.001-30	0.001	AA, UA	Synthetic Urine	[87]
TiN-rGO/GCE	DPV	0.016 5-175	0.159	AA, UA, NaCl, $MgSO_4$, KNO_3, Nas_2SO_3, CYS, GLU, Alanine, TYR	Urine	[88]
CS film/ZnO NPs@C	DPV	0.76 0.00012-152	0.00004	GLU, AA, UA, LAC, P-PD, O-PD, H_2O_2, NaCl	NS	[89]
Fe_3O_4-Gr	DPV	1.61 5-160	0.75	UA, AC	PHY.SA	[90]
Ag@HCSs	CH	0.76 3-2000	0.6	AA, H_2O_2, UA, GLY, GLU	Serum	[91]
Ni-MOF	DPV	0.285* 0.2-100	0.06	AA, UA, Ca^{2+}, K^+, Na^+, CYST	DA HYD	[92]
MoOx NPs/SPCE	SWV	6.78* 0.1–600	0.043	GLU, AA, UA, FC, KCl, NaCl	NS	[93]
CNT- micropillary array	DPV	25.59* 0.001-0.06	0.00077	GLU, AA, UA, 5-HT	NS	[94]
rGO/MWCNT/PPy	CH	8.96 0.025-1	0.023	DA, AA, UA, NEP, EP	NS	[95]

Nanostructured CuSe	SWV	26.8 0.25-10	0.098	AA, UA, GLU, NaCl	Urine	[96]
MWCNT/Au/GCE	DPV	0.1216 0.7-108	0.21	K^+, Na^+, Mg^{2+}, Zn^{2+}, Cl^-, HCO_3^-, SO_4^{2-}, NO_3^-, glutamate, AA, β-CD, leucine, NADH, CA, GLIU	Urine	[97]
CdSe/CdS quantum dots	DPV	0.2* 0.5-15	0.096	KCl, NaCl, AA, acetaminophen AC, UA	Serum	[98]
AuNPs-rGO-ITO	**SWV**	**6.02** ***0.1 –20***	**0.075**	**UA, AA**	**Real and Synthetic Urine**	**This Work**
PtNPs-rGO-ITO	**SWV**	**7.19** ***0.1 –10***	**0.062**	**UA, AA**	**Synthetic Urine**	**This Work**

4 Conclusions

Dopamine was electrochemically detected using sensors fabricated from an ITO-PET substrate covered with AuNPs-rGO or PtNPs-rGO. ITO-PET substrates were coated by electro co-deposition of rGO and MtNPs from a solution containing GO and metal precursor. The formation of metal NPs and rGO was confirmed by FESEM, XRD, Raman and XPS. CVs at different scar rates were performed showing that the MtNPs-rGO-ITO electrodes present the highest specific capacitance and thus the highest electrochemical active surface area. The main electrodeposition parameters (applied potential, solution composition and deposition time) were optimized in order to increase the sensor performances towards dopamine detection. In particular, the best performances were achieved with electrodes obtained at -0.8 V *vs.* SCE, using ABS buffer solution containing 0.25 mM of metal precursor, 0.5 mg/mL of GO and for 200 s for rGO-Au-NPs or 300 s for PtNPs-rGO-ITO based sensors. Using these conditions, for AuNPs-rGO-ITO based sensors, a linear range from 0.1 µM up to 20 µM, with a sensitivity of 6.02 µA μM^{-1} cm^{-2} and LOD of 75 nM was obtained. For PtNPs-rGO-ITO based sensors, the linear range is from 0.1 to 10 µM of DA with a sensitivity of

7.19 µA μM^{-1} cm^{-2}, with an esteemed LOD of 62 nM. The high sensitivity of Pt NPs is due to the higher catalytic activity of Pt towards DA oxidation in comparison to Au. It is important to highlight that, for both electrodes the measured LOD values are significantly lower than expected DA concentrations in real urine samples (about 600 nM).

The electrode selectivity towards ascorbic and uric acid was studied. No interference was found from ascorbic acid even at high concentration due to the electrostatic repulsion between GO and the ascorbic acid. In the case of uric acid, a negligible interference was found only at high concentrations causing a loss in sensor detection of ~ 8%.

The excellent performance of the sensor can be attributable mainly to the very good electrocatalytic properties of rGO towards the DA detection, and also to the nanostructured morphology of the sensor surface. In fact, a nanostructured surface ensures a high electrochemically active surface area, characterized by a large number of active sites where the DA oxidation can take place. The electrodes show excellent behaviour even after being bent and stretched, while excessive twisting causes a drastic drop in performance.

Synthetic urine was used to study the performance of the sensors for dopamine detection. In this media, in comparison to the value obtained for PBS, a lower sensitivity of 3.365 µA μM^{-1} cm^{-2} was obtained. In any case, the sensitivity of our proposed sensors is still higher when compared to other electrochemical sensors for DA. In fact, only in few articles, values higher than 1 µA μM^{-1} cm^{-2} were reached.

Sensors were also validated in real urine samples and the results were very close to those obtained using a standard HPLC method with a recovery of about 94%.

Results herein presented are of great importance because they support the possibility for DA detection using electrodes obtained with a very simple and low-cost preparation method with short fabrication times. These features make this sensor easily scalable and therefore applicable in research laboratories to substitute current expensive and time-consuming approaches.

ACKNOWLEDGMENTS

This work was supported by University of Palermo and Italian National Research Council, and has been partially financed by the Project "PATCHES – Patient-Centered HEalthcare System for neurodegenerative diseases" (n. 610, Ministero dello Sviluppo Economico, Accordi per l'innovazione, Programma operativo nazionale «Imprese e competitività» 2014-2020 FESR e del Fondo per la crescita sostenibile) and by a research grant for the VistaMilk Centre Science Foundation Ireland (SFI); Department of Agriculture, Food and the Marine (DAFM) under Grant Number 16/RC/3835

REFERENCE

[1] J.L.W. Bosboom, D. Stoffers, E.C. Wolters, The role of acetylcholine and dopamine in dementia and psychosis in Parkinson's disease, J. Neural Transm. Suppl. (2003) 185–195. https://doi.org/10.1007/978-3-7091-0643-3_11.

[2] O.L. Lopez, S.R. Wisnieski, J.T. Becker, F. Boiler, S.T. DeKosky, Extrapyramidal Signs in Patients With Probable Alzheimer Disease, Archives of Neurology. 54 (1997) 969–975. https://doi.org/10.1001/archneur.1997.00550200033007.

[3] A. Martorana, G. Koch, Is dopamine involved in Alzheimer's disease?, Front Aging Neurosci. 6 (2014) 252. https://doi.org/10.3389/fnagi.2014.00252.

[4] J. Weller, A. Budson, Current understanding of Alzheimer’s disease diagnosis and treatment, F1000Res. 7 (2018) 1161. https://doi.org/10.12688/f1000research.14506.1.

[5] J. Jankovic, Parkinson’s disease: clinical features and diagnosis, Journal of Neurology, Neurosurgery & Psychiatry. 79 (2008) 368–376. https://doi.org/10.1136/jnnp.2007.131045.

[6] V.A. Harpin, The effect of ADHD on the life of an individual, their family, and community from preschool to adult life, Archives of Disease in Childhood. 90 (2005) i2–i7. https://doi.org/10.1136/adc.2004.059006.

[7] S. Kar, S.P.M. Slowikowski, D. Westaway, H.T.J. Mount, Interactions between beta-amyloid and central cholinergic neurons: implications for Alzheimer’s disease, J Psychiatry Neurosci. 29 (2004) 427–441.

[8] R.B. Mailman, D.W. Schulz, C.D. Kilts, M.H. Lewis, H. Rollema, S. Wyrick, The Multiplicity of the D1 Dopamine Receptor, in: G.R. Breese, I. Creese (Eds.), Neurobiology of Central D1-Dopamine Receptors, Springer US, Boston, MA, 1986: pp. 53–72. https://doi.org/10.1007/978-1-4684-5191-7_4.

[9] S.M. Namkung, J.S. Choi, J.H. Park, M.G. Yang, M.W. Lee, S.W. Kim, Detection of Dopamine and Serotonin by Competitive Enzyme-Linked Immunosorbent Assay, Korean J Clin Lab Sci. 49 (2017) 220–226. https://doi.org/10.15324/kjcls.2017.49.3.220.

[10] H.-X. Zhao, H. Mu, Y.-H. Bai, H. Yu, Y.-M. Hu, A rapid method for the determination of dopamine in porcine muscle by pre-column derivatization and HPLC with fluorescence detection, Journal of Pharmaceutical Analysis. 1 (2011) 208–212. https://doi.org/10.1016/j.jpha.2011.04.003.

[11] F.B. Kamal Eddin, Y. Wing Fen, Recent Advances in Electrochemical and Optical Sensing of Dopamine, Sensors. 20 (2020) 1039. https://doi.org/10.3390/s20041039.

[12] L.A. Wasiewska, I. Seymour, B. Patella, R. Inguanta, C.M. Burgess, G. Duffy, A. O’Riordan, Reagent free electrochemical-based detection of silver ions at interdigitated microelectrodes using in-situ pH control, Sensors and Actuators B: Chemical. (2021) 129531. https://doi.org/10.1016/j.snb.2021.129531.

[13] X. Liu, J. Liu, Biosensors and sensors for dopamine detection, View. 2 (2021) 20200102. https://doi.org/10.1002/VIW.20200102.

[14] S. Cogal, A review of poly(3,4-ethylenedioxythiophene) and its composites-based electrochemical sensors for dopamine detection, Polymer-Plastics Technology and Materials. 60 (2021) 345–357. https://doi.org/10.1080/25740881.2020.1811321.

[15] B. Patella, R.R. Russo, A. O’Riordan, G. Aiello, C. Sunseri, R. Inguanta, Copper nanowire array as highly selective electrochemical sensor of nitrate ions in water, Talanta. 221 (2021) 121643. https://doi.org/10.1016/j.talanta.2020.121643.

[16] A.J. Bandodkar, J. Wang, Non-invasive wearable electrochemical sensors: a review, Trends in Biotechnology. 32 (2014) 363–371. https://doi.org/10.1016/j.tibtech.2014.04.005.

[17] P.C. Ferreira, V.N. Ataíde, C.L. Silva Chagas, L. Angnes, W.K. Tomazelli Coltro, T.R. Longo Cesar Paixão, W. Reis de Araujo, Wearable electrochemical sensors for forensic and clinical applications, TrAC Trends in Analytical Chemistry. 119 (2019) 115622. https://doi.org/10.1016/j.trac.2019.115622.

[18] A. Murphy, I. Seymour, J. Rohan, A. O'Riordan, I. O'Connell, Portable Data Acquisition System for Nano and Ultra-Micro Scale Electrochemical Sensors, IEEE Sensors J. (2020) 1–1. https://doi.org/10.1109/JSEN.2020.3021941.

[19] M. Ouellette, J. Mathault, S.D. Niyonambaza, A. Miled, E. Boisselier, Electrochemical Detection of Dopamine Based on Functionalized Electrodes, Coatings. 9 (2019) 496. https://doi.org/10.3390/coatings9080496.

[20] Bernardo Patella, Rosalinda Inguanta, Salvatore Piazza, Carmelo Sunseri, Nanowire ordered arrays for electrochemical sensing of h2o2, Chemical Engineering Transactions. 47 (2016) 19–24. https://doi.org/10.3303/CET1647004.

[21] C. Barrett, F. O'Sullivan, S. Barry, K. Grygoryev, D. O'Gorman, C. O'Mahony, A. O'Riordan, Novel Surface Modified Polymer Microneedle based Biosensors for Interstitial Fluid Glucose Detection, in: 2019 IEEE SENSORS, IEEE, Montreal, QC, Canada, 2019: pp. 1–4. https://doi.org/10.1109/SENSORS43011.2019.8956509.

[22] H. Liu, C. Zhao, Wearable electrochemical sensors for noninvasive monitoring of health—a perspective, Current Opinion in Electrochemistry. 23 (2020) 42–46. https://doi.org/10.1016/j.coelec.2020.03.008.

[23] B. Patella, A. Sortino, G. Aiello, C. Sunseri, R. Inguanta, Reduced graphene oxide decorated with metals nanoparticles electrode as electrochemical sensor for dopamine, in: 2019 IEEE International Conference on Flexible and Printable Sensors and Systems (FLEPS), IEEE, Glasgow, United Kingdom, 2019: pp. 1–3. https://doi.org/10.1109/FLEPS.2019.8792267.

[24] Y. Li, Q. Lu, A. Shi, Y. Chen, S. Wu, L. Wang, Electrochemical Determination of Dopamine in the Presence of Ascorbic Acid and Uric Acid Using the Synergistic Effect of Gold Nanoflowers and L-Cysteamine Monolayer at the Surface of a Gold Electrode, Anal. Sci. 27 (2011) 921. https://doi.org/10.2116/analsci.27.921.

[25] F. Mazzara, B. Patella, G. Aiello, C. Sunseri, R. Inguanta, Ascorbic Acid determination using linear sweep voltammetry on flexible electrode modified with gold nanoparticles and reduced graphene oxide, in: 2020 IEEE 20th Mediterranean Electrotechnical Conference (MELECON), IEEE, Palermo, Italy, 2020: pp. 406–410. https://doi.org/10.1109/MELECON48756.2020.9140684.

[26] M.Z.H. Khan, Graphene Oxide Modified Electrodes for Dopamine Sensing, Journal of Nanomaterials. 2017 (2017) 1–11. https://doi.org/10.1155/2017/8178314.

[27] A. Pandikumar, G.T. Soon How, T.P. See, F.S. Omar, S. Jayabal, K.Z. Kamali, N. Yusoff, A. Jamil, R. Ramaraj, S.A. John, H.N. Lim, N.M. Huang, Graphene and its nanocomposite material based electrochemical sensor platform for dopamine, RSC Adv. 4 (2014) 63296–63323. https://doi.org/10.1039/C4RA13777A.

[28] J.N. Appaturi, T. Pulingam, S. Muniandy, I.J. Dinshaw, L.B. Fen, Mohd.R. Johan, Supported cobalt nanoparticles on graphene oxide/mesoporous silica for oxidation of phenol and electrochemical detection of H2O2 and Salmonella spp, Materials Chemistry and Physics. 232 (2019) 493–505. https://doi.org/10.1016/j.matchemphys.2018.12.025.

[29] A. Bonanni, M. Pumera, Graphene Platform for Hairpin-DNA-Based Impedimetric Genosensing, ACS Nano. 5 (2011) 2356–2361. https://doi.org/10.1021/nn200091p.

[30] Z. Miao, D. Zhang, Q. Chen, Non-enzymatic Hydrogen Peroxide Sensors Based on Multi-wall Carbon Nanotube/Pt Nanoparticle Nanohybrids, Materials. 7 (2014) 2945–2955. https://doi.org/10.3390/ma7042945.

[31] S. Berbeć, S. Żołądek, A. Jabłońska, B. Pałys, Electrochemically reduced graphene oxide on gold nanoparticles modified with a polyoxomolybdate film. Highly sensitive non-enzymatic electrochemical detection of H2O2, Sensors and Actuators B: Chemical. 258 (2018) 745–756. https://doi.org/10.1016/j.snb.2017.11.163.

[32] P. Bollella, G. Fusco, C. Tortolini, G. Sanzò, G. Favero, L. Gorton, R. Antiochia, Beyond graphene: Electrochemical sensors and biosensors for biomarkers detection, Biosensors and Bioelectronics. 89 (2017) 152–166. https://doi.org/10.1016/j.bios.2016.03.068.

[33] X.-Z. Tang, X. Li, Z. Cao, J. Yang, H. Wang, X. Pu, Z.-Z. Yu, Synthesis of graphene decorated with silver nanoparticles by simultaneous reduction of graphene oxide and silver ions with glucose, Carbon. 59 (2013) 93–99. https://doi.org/10.1016/j.carbon.2013.02.058.

[34] S. Bahrani, Z. Razmi, M. Ghaedi, A. Asfaram, H. Javadian, Ultrasound-accelerated synthesis of gold nanoparticles modified choline chloride functionalized graphene oxide as a novel sensitive bioelectrochemical sensor: Optimized meloxicam detection using CCD-RSM design and application for human plasma sample, Ultrasonics Sonochemistry. 42 (2018) 776–786. https://doi.org/10.1016/j.ultsonch.2017.12.042.

[35] M.A. Kumar, V. Lakshminarayanan, S.S. Ramamurthy, Platinum nanoparticles–decorated graphene-modified glassy carbon electrode toward the electrochemical determination of ascorbic acid, dopamine, and paracetamol, Comptes Rendus Chimie. 22 (2019) 58–72. https://doi.org/10.1016/j.crci.2018.09.015.

[36] M. Baghayeri, H. Alinezhad, M. Tarahomi, M. Fayazi, M. Ghanei-Motlagh, B. Maleki, A non-enzymatic hydrogen peroxide sensor based on dendrimer functionalized magnetic graphene oxide decorated with palladium nanoparticles, Applied Surface Science. 478 (2019) 87–93. https://doi.org/10.1016/j.apsusc.2019.01.201.

[37] M. Guler, Y. Dilmac, Palladium nanoparticles decorated (3-aminopropyl)triethoxysilane functionalized reduced graphene oxide for electrochemical determination of glucose and hydrogen peroxide, Journal of Electroanalytical Chemistry. 834 (2019) 49–55. https://doi.org/10.1016/j.jelechem.2018.12.052.

[38] A.V. Kukhta, A.G. Paddubskaya, P.P. Kuzhir, S.A. Maksimenko, S.A. Vorobyova, S. Bistarelli, A. Cataldo, S. Bellucci, Copper nanoparticles decorated graphene nanoplatelets and composites with PEDOT:PSS, Synthetic Metals. 222 (2016) 192–197. https://doi.org/10.1016/j.synthmet.2016.10.006.

[39] C.-S. Lee, S. Yu, T. Kim, One-Step Electrochemical Fabrication of Reduced Graphene Oxide/Gold Nanoparticles Nanocomposite-Modified Electrode for Simultaneous Detection of Dopamine, Ascorbic Acid, and Uric Acid, Nanomaterials. 8 (2017) 17. https://doi.org/10.3390/nano8010017.

[40] G. Yu, W. Wu, X. Pan, Q. Zhao, X. Wei, Q. Lu, High Sensitive and Selective Sensing of Hydrogen Peroxide Released from Pheochromocytoma Cells Based on Pt-Au Bimetallic Nanoparticles Electrodeposited on Reduced Graphene Sheets, Sensors. 15 (2015) 2709–2722. https://doi.org/10.3390/s150202709.

[41] Q. Lan, C. Ren, A. Lambert, G. Zhang, J. Li, Q. Cheng, X. Hu, Z. Yang, Platinum Nanoparticle-decorated Graphene Oxide@Polystyrene Nanospheres for Label-free Electrochemical Immunosensing of Tumor Markers, ACS Sustainable Chem. Eng. 8 (2020) 4392–4399. https://doi.org/10.1021/acssuschemeng.9b06858.

[42] Y.J. Yang, W. Li, Gold nanoparticles/graphene oxide composite for electrochemical sensing of hydroxylamine and hydrogen peroxide, Fullerenes, Nanotubes and Carbon Nanostructures. 26 (2018) 195–

204. https://doi.org/10.1080/1536383X.2018.1424711.

[43] T.K. Sari, F. Takahashi, J. Jin, R. Zein, E. Munaf, Electrochemical Determination of Chromium(VI) in River Water with Gold Nanoparticles–Graphene Nanocomposites Modified Electrodes, Anal. Sci. 34 (2018) 155–160. https://doi.org/10.2116/analsci.34.155.

[44] Z. Yu, Electrodeposition of Gold Nanoparticles on Electrochemically Reduced Graphene Oxide for High Performance Supercapacitor Electrode Materials, Int. J. Electrochem. Sci. (2016) 3643–3650. https://doi.org/10.20964/110448.

[45] C. Sun, F. Li, H. An, Z. Li, A.M. Bond, J. Zhang, Facile electrochemical co-deposition of metal (Cu, Pd, Pt, Rh) nanoparticles on reduced graphene oxide for electrocatalytic reduction of nitrate/nitrite, Electrochimica Acta. 269 (2018) 733–741. https://doi.org/10.1016/j.electacta.2018.03.005.

[46] X. Cui, X. Fang, H. Zhao, Z. Li, H. Ren, An electrochemical sensor for dopamine based on polydopamine modified reduced graphene oxide anchored with tin dioxide and gold nanoparticles, Anal. Methods. 9 (2017) 5322–5332. https://doi.org/10.1039/C7AY00991G.

[47] B. Patella, M. Buscetta, S. Di Vincenzo, M. Ferraro, G. Aiello, C. Sunseri, E. Pace, R. Inguanta, C. Cipollina, Electrochemical sensor based on rGO/Au nanoparticles for monitoring H2O2 released by human macrophages, Sensors and Actuators B: Chemical. 327 (2021) 128901. https://doi.org/10.1016/j.snb.2020.128901.

[48] Y. Shen, M.Y. Ye, Determination of the Stability of Dopamine in Aqueous Solutions by High Performance Liquid Chromatography, Journal of Liquid Chromatography. 17 (1994) 1557–1565. https://doi.org/10.1080/10826079408013178.

[49] A.E. Sánchez-Rivera, S. Corona-Avendaño, G. Alarcón-Angeles, A. Rojas-Hernández, M.T. Ramírez-Silva, M.A. Romero-Romo, Spectrophotometric study on the stability of dopamine and the determination of its acidity constants, Spectrochimica Acta Part A: Molecular and Biomolecular Spectroscopy. 59 (2003) 3193–3203. https://doi.org/10.1016/S1386-1425(03)00138-0.

[50] M. Battaglia, S. Piazza, C. Sunseri, R. Inguanta, Amorphous silicon nanotubes via galvanic displacement deposition, Electrochemistry Communications. 34 (2013) 134–137. https://doi.org/10.1016/j.elecom.2013.05.041.

[51] F. Ganci, S. Lombardo, C. Sunseri, R. Inguanta, Nanostructured electrodes for hydrogen production in alkaline electrolyzer, Renewable Energy. 123 (2018) 117–124. https://doi.org/10.1016/j.renene.2018.02.033.

[52] L. Silipigni, F. Barreca, E. Fazio, F. Neri, T. Spanò, S. Piazza, C. Sunseri, R. Inguanta, Template Electrochemical Growth and Properties of Mo Oxide Nanostructures, J. Phys. Chem. C. 118 (2014) 22299–22308. https://doi.org/10.1021/jp505819j.

[53] F. Mazzara, B. Patella, C. D'Agostino, M.G. Bruno, S. Carbone, F. Lopresti, G. Aiello, C. Torino, A. Vilasi, A. O'Riordan, R. Inguanta, PANI-Based Wearable Electrochemical Sensor for pH Sweat Monitoring, Chemosensors. 9 (2021) 169. https://doi.org/10.3390/chemosensors9070169.

[54] Patella B., Piazza S., Sunseri C., Inguanta R., Nio thin film for mercury detection in water by square wave anodic stripping voltammetry, Chemical Engineering Transactions. 60 (2017) 1–6. https://doi.org/10.3303/CET1760001.

[55] Rosalinda Inguanta, Germano Ferrara, Salvatore Piazza, Carmelo Sunseri, Nanostructure fabrication

by template deposition into anodic alumina membranes, Chemical Engineering Transactions. 17 (2009) 957–962. https://doi.org/10.3303/CET0917160.

[56] S. Pruneanu, A.R. Biris, F. Pogacean, C. Socaci, M. Coros, M.C. Rosu, F. Watanabe, A.S. Biris, The influence of uric and ascorbic acid on the electrochemical detection of dopamine using graphene-modified electrodes, Electrochimica Acta. 154 (2015) 197–204. https://doi.org/10.1016/j.electacta.2014.12.046.

[57] M. Sajid, M.K. Nazal, M. Mansha, A. Alsharaa, S.M.S. Jillani, C. Basheer, Chemically modified electrodes for electrochemical detection of dopamine in the presence of uric acid and ascorbic acid: A review, TrAC Trends in Analytical Chemistry. 76 (2016) 15–29. https://doi.org/10.1016/j.trac.2015.09.006.

[58] M. Zhou, Y. Wang, Y. Zhai, J. Zhai, W. Ren, F. Wang, S. Dong, Controlled Synthesis of Large-Area and Patterned Electrochemically Reduced Graphene Oxide Films, Chem. Eur. J. 15 (2009) 6116–6120. https://doi.org/10.1002/chem.200900596.

[59] G. Gotti, K. Fajerwerg, D. Evrard, P. Gros, Electrodeposited gold nanoparticles on glassy carbon: Correlation between nanoparticles characteristics and oxygen reduction kinetics in neutral media, Electrochimica Acta. 128 (2014) 412–419. https://doi.org/10.1016/j.electacta.2013.10.172.

[60] S.S. Shereema RM, Electrochemical Detection of Dopamine in Presence of Serotonin and Ascorbic acid at Tetraoctyl ammonium bromide Modified Carbon Paste Electrode: A Voltammetric Study, J Biosens Bioelectron. 06 (2015). https://doi.org/10.4172/2155-6210.1000168.

[61] J. Wang, B. Li, Z. Li, K. Ren, L. Jin, S. Zhang, H. Chang, Y. Sun, J. Ji, Electropolymerization of dopamine for surface modification of complex-shaped cardiovascular stents, Biomaterials. 35 (2014) 7679–7689. https://doi.org/10.1016/j.biomaterials.2014.05.047.

[62] X. Cao, Y. Ye, S. Liu, Gold nanoparticle-based signal amplification for biosensing, Analytical Biochemistry. 417 (2011) 1–16. https://doi.org/10.1016/j.ab.2011.05.027.

[63] P. Connor, J. Schuch, B. Kaiser, W. Jaegermann, The Determination of Electrochemical Active Surface Area and Specific Capacity Revisited for the System MnO $_x$ as an Oxygen Evolution Catalyst, Zeitschrift Für Physikalische Chemie. 234 (2020) 979–994. https://doi.org/10.1515/zpch-2019-1514.

[64] B. Wang, X. Ji, J. Ren, R. Ni, L. Wang, Enhanced electrocatalytic activity of graphene-gold nanoparticles hybrids for peroxynitrite electrochemical detection on hemin-based electrode, Bioelectrochemistry. 118 (2017) 75–82. https://doi.org/10.1016/j.bioelechem.2017.07.005.

[65] G. Gotti, K. Fajerwerg, D. Evrard, P. Gros, Electrodeposited gold nanoparticles on glassy carbon: Correlation between nanoparticles characteristics and oxygen reduction kinetics in neutral media, Electrochimica Acta. 128 (2014) 412–419. https://doi.org/10.1016/j.electacta.2013.10.172.

[66] M. Zhou, Y. Wang, Y. Zhai, J. Zhai, W. Ren, F. Wang, S. Dong, Controlled Synthesis of Large-Area and Patterned Electrochemically Reduced Graphene Oxide Films, Chem. Eur. J. 15 (2009) 6116–6120. https://doi.org/10.1002/chem.200900596.

[67] E. Topçu, K. Dağcı Kıranşan, Flexible gold nanoparticles/rGO and thin film/rGO papers: novel electrocatalysts for hydrogen evolution reaction, J. Chem. Technol. Biotechnol. 94 (2019) 3895–3904. https://doi.org/10.1002/jctb.6187.

[68] Patella, B, Buscetta, M, Di Vincenzo, S, Ferraro, M., Aiello, G, Sunseri, C, Pace, E, Inguanta, R., Cipollina, C., Electrochemical sensor based on r-GO/Au nanoparticles for monitoring H2O2 released by human macrophages, Sensors and Actuators B: Chemical. Under Revision (2020).

[69] E.A. Chiticaru, L. Pilan, C.-M. Damian, E. Vasile, J.S. Burns, M. Ioniţă, Influence of Graphene Oxide Concentration when Fabricating an Electrochemical Biosensor for DNA Detection, Biosensors. 9 (2019) 113. https://doi.org/10.3390/bios9040113.

[70] D. Mohanadas, M.A.A. Mohd Abdah, N.H.N. Azman, T.B.S.A. Ravoof, Y. Sulaiman, Facile synthesis of PEDOT-rGO/HKUST-1 for high performance symmetrical supercapacitor device, Sci Rep. 11 (2021) 11747. https://doi.org/10.1038/s41598-021-91100-x.

[71] S. Fang, D. Huang, R. Lv, Y. Bai, Z.-H. Huang, J. Gu, F. Kang, Three-dimensional reduced graphene oxide powder for efficient microwave absorption in the S-band (2–4 GHz), RSC Adv. 7 (2017) 25773–25779. https://doi.org/10.1039/C7RA03215C.

[72] A.R. West, Solid state chemistry and its applications, Second edition, student edition, Wiley, Chichester, West Sussex, UK, 2014.

[73] L. Stobinski, B. Lesiak, A. Malolepszy, M. Mazurkiewicz, B. Mierzwa, J. Zemek, P. Jiricek, I. Bieloshapka, Graphene oxide and reduced graphene oxide studied by the XRD, TEM and electron spectroscopy methods, Journal of Electron Spectroscopy and Related Phenomena. 195 (2014) 145–154. https://doi.org/10.1016/j.elspec.2014.07.003.

[74] D.H. Ha, S. Jung, H.-J. Kim, D. Kim, W.-J. Kim, S.N. Yi, Y. Jun, Y.J. Yun, Transition of graphene oxide-coated fiber bundles from insulator to conductor by chemical reduction, Synthetic Metals. 204 (2015) 90–94. https://doi.org/10.1016/j.synthmet.2015.03.018.

[75] G.K. Ramesha, S. Sampath, Electrochemical Reduction of Oriented Graphene Oxide Films: An in Situ Raman Spectroelectrochemical Study, J. Phys. Chem. C. 113 (2009) 7985–7989. https://doi.org/10.1021/jp811377n.

[76] M.P. Casaletto, A. Longo, A. Martorana, A. Prestianni, A.M. Venezia, XPS study of supported gold catalysts: the role of Au0 and Au+δ species as active sites, Surf. Interface Anal. 38 (2006) 215–218. https://doi.org/10.1002/sia.2180.

[77] G. Jena, S. Sofia, B. Anandkumar, S.C. Vanithakumari, R.P. George, J. Philip, Graphene oxide/polyvinylpyrrolidone composite coating on 316L SS with superior antibacterial and anti-biofouling properties, Progress in Organic Coatings. 158 (2021) 106356. https://doi.org/10.1016/j.porgcoat.2021.106356.

[78] D. Minta, A. Moyseowicz, S. Gryglewicz, G. Gryglewicz, A Promising Electrochemical Platform for Dopamine and Uric Acid Detection Based on a Polyaniline/Iron Oxide-Tin Oxide/Reduced Graphene Oxide Ternary Composite, Molecules. 25 (2020) 5869. https://doi.org/10.3390/molecules25245869.

[79] G. Gauglitz, Analytical evaluation of sensor measurements, Anal Bioanal Chem. 410 (2018) 5–13. https://doi.org/10.1007/s00216-017-0624-z.

[80] An Electrochemical Sensor Based on Platinum Nanoparticles and Mesoporous Carbon Composites for Selective Analysis of Dopamine, Int. J. Electrochem. Sci. (2019) 1082–1091. https://doi.org/10.20964/2019.01.112.

[81] Y. Dalmaz, L. Peyrin, L. Sann, J. Dutruge, Age-related changes in catecholamine metabolites of human urine from birth to adulthood, J. Neural Transmission. 46 (1979) 153–174. https://doi.org/10.1007/BF01250336.

[82] O.E. Fayemi, A.S. Adekunle, B.E. Kumara Swamy, E.E. Ebenso, Electrochemical sensor for the

detection of dopamine in real samples using polyaniline/NiO, ZnO, and Fe3O4 nanocomposites on glassy carbon electrode, Journal of Electroanalytical Chemistry. 818 (2018) 236–249. https://doi.org/10.1016/j.jelechem.2018.02.027.

[83] Q. Gong, H. Han, Y. Wang, C. Yao, H. Yang, J. Qiao, An electrochemical sensor for dopamine detection based on the electrode of a poly-tryptophan-functionalized graphene composite, New Carbon Materials. 35 (2020) 34–41. https://doi.org/10.1016/S1872-5805(20)60473-5.

[84] B. Demirkan, S. Bozkurt, K. Cellat, K. Arıkan, M. Yılmaz, A. Şavk, M.H. Çalımlı, M.S. Nas, M.N. Atalar, M.H. Alma, F. Sen, Palladium supported on polypyrrole/reduced graphene oxide nanoparticles for simultaneous biosensing application of ascorbic acid, dopamine, and uric acid, Sci Rep. 10 (2020) 2946. https://doi.org/10.1038/s41598-020-59935-y.

[85] H. Zhang, S. Liu, Electrochemical sensors based on nitrogen-doped reduced graphene oxide for the simultaneous detection of ascorbic acid, dopamine and uric acid, Journal of Alloys and Compounds. 842 (2020) 155873. https://doi.org/10.1016/j.jallcom.2020.155873.

[86] K. Kunpatee, S. Traipop, O. Chailapakul, S. Chuanuwatanakul, Simultaneous determination of ascorbic acid, dopamine, and uric acid using graphene quantum dots/ionic liquid modified screen-printed carbon electrode, Sensors and Actuators B: Chemical. 314 (2020) 128059. https://doi.org/10.1016/j.snb.2020.128059.

[87] W. Ji, D. Wu, W. Tang, X. Xi, Y. Su, X. Guo, R. Liu, Carbonized silk fabric-based flexible organic electrochemical transistors for highly sensitive and selective dopamine detection, Sensors and Actuators B: Chemical. 304 (2020) 127414. https://doi.org/10.1016/j.snb.2019.127414.

[88] J. Feng, Q. Li, J. Cai, T. Yang, J. Chen, X. Hou, Electrochemical detection mechanism of dopamine and uric acid on titanium nitride-reduced graphene oxide composite with and without ascorbic acid, Sensors and Actuators B: Chemical. 298 (2019) 126872. https://doi.org/10.1016/j.snb.2019.126872.

[89] Y. Song, J. Han, L. Xu, L. Miao, C. Peng, L. Wang, A dopamine-imprinted chitosan Film/Porous ZnO NPs@carbon Nanospheres/Macroporous carbon for electrochemical sensing dopamine, Sensors and Actuators B: Chemical. 298 (2019) 126949. https://doi.org/10.1016/j.snb.2019.126949.

[90] G. Venkataprasad, T. Madhusudana Reddy, A. Lakshmi Narayana, O.M. Hussain, P. Shaikshavali, T. Venu Gopal, P. Gopal, A facile synthesis of Fe3O4-Gr nanocomposite and its effective use as electrochemical sensor for the determination of dopamine and as anode material in lithium ion batteries, Sensors and Actuators A: Physical. 293 (2019) 87–100. https://doi.org/10.1016/j.sna.2019.04.035.

[91] X. Zhang, J. Zheng, Hollow carbon sphere supported Ag nanoparticles for promoting electrocatalytic performance of dopamine sensing, Sensors and Actuators B: Chemical. 290 (2019) 648–655. https://doi.org/10.1016/j.snb.2019.04.040.

[92] Z. Huang, L. Zhang, P. Cao, N. Wang, M. Lin, Electrochemical sensing of dopamine using a Ni-based metal-organic framework modified electrode, Ionics. 27 (2021) 1339–1345. https://doi.org/10.1007/s11581-020-03857-2.

[93] E. Fazio, S. Spadaro, M. Bonsignore, N. Lavanya, C. Sekar, S.G. Leonardi, G. Neri, F. Neri, Molybdenum oxide nanoparticles for the sensitive and selective detection of dopamine, Journal of Electroanalytical Chemistry. 814 (2018) 91–96. https://doi.org/10.1016/j.jelechem.2018.02.051.

[94] A.-Y. Chang, X. Liu, Y. Pei, C. Gong, P.U. Arumugam, S. Wang, Dopamine sensing with robust

carbon nanotube implanted polymer micropillar array electrodes fabricated by coupling micromolding and infiltration coating processes, Electrochimica Acta. 368 (2021) 137632. https://doi.org/10.1016/j.electacta.2020.137632.

[95] V. Kathiresan, D. Thirumalai, T. Rajarathinam, M. Yeom, J. Lee, S. Kim, J.-H. Yoon, S.-C. Chang, A simple one-step electrochemical deposition of bioinspired nanocomposite for the non-enzymatic detection of dopamine, J Anal Sci Technol. 12 (2021) 5. https://doi.org/10.1186/s40543-021-00260-y.

[96] S. Umapathi, J. Masud, H. Coleman, M. Nath, Electrochemical sensor based on CuSe for determination of dopamine, Microchim Acta. 187 (2020) 440. https://doi.org/10.1007/s00604-020-04405-5.

[97] Q. Guan, H. Guo, R. Xue, M. Wang, X. Zhao, T. Fan, W. Yang, M. Xu, W. Yang, Electrochemical sensor based on covalent organic frameworks-MWCNT-NH2/AuNPs for simultaneous detection of dopamine and uric acid, Journal of Electroanalytical Chemistry. 880 (2021) 114932. https://doi.org/10.1016/j.jelechem.2020.114932.

[98] C.C.L. de França, D. Meneses, A.C.A. Silva, N.O. Dantas, F.C. de Abreu, J.M. Petroni, B.G. Lucca, Development of novel paper-based electrochemical device modified with CdSe/CdS magic-sized quantum dots and application for the sensing of dopamine, Electrochimica Acta. 367 (2021) 137486. https://doi.org/10.1016/j.electacta.2020.137486.

GRAPHICAL ABSTRACT